An Adjoint Ocean Model Using Finite Elements: An Application to the South Atlantic

Uwe Dobrindt[1,2] **and Jens Schröter**[1]

[1]Alfred Wegener Institute for Polar and Marine Research

Postfach 12 01 61, D-27515 Bremerhaven, Germany

[2]STN Atlas Elektronik GmbH

Sebaldsbrücker Heerstr. 238, D-28305 Bremen, Germany

e-mail: dobrindt@stn-atlas.de, jschroeter@awi-bremerhaven.de

Submitted to J. Atmos. Oceanic Technol.

06. September 2000

Revised 11. December 2000, 2nd Revised 12. June 2001

Abstract

A new inverse model to study the large scale ocean circulation and its associated heat and fresh water budget is developed. The model relies on traditional assumptions of mass, heat and salt conservation. A 3-dimensional velocity field which is in steady state and obeys geostrophy is derived. Using this flow field, the steady state advection-diffusion equations for temperature and salinity are solved and the corresponding density is calculated. An optimization approach is used that adjusts reference velocities to get model parameters close to observations and that the velocities are in geostrophic balance with the model density field. In order to allow a variable spatial resolution, the finite element method is used. The mesh is totally unstructured and the 3-dimensional elements are tetrahedra.

Climatological hydrographic data, observations of sea surface height (SSH) from satellite altimetry and wind data are assimilated in the model. The advantages of the finite element method make it possible to use an easy representation of the model parameters on the tetrahedra. It is not difficult to find the adjoint form of the discrete equations. The unstructured mesh agrees well with the complex geometry of the bottom topography.

The model is applied to the South Atlantic. First model results show, that the upper-level circulation corresponds to the circulation known from literature. The volume transport through Drake Passage is constrained to be 130 Sv. The transports of water masses, heat and salt across the open boundaries (Drake Passage, 30°S, 20°E) are in agreement with the literature. The formation rate of bottom water is 13.0 Sv and the heat transport across 30°S to the north is 0.64 PW.

1 Introduction

Describing the global ocean circulation is still a problem despite of more than hundred years of systematic observation and research in oceanography. The large scale transport and the distribution of water masses can be derived from hydrographic data (temperature and salinity) using the geostrophic equations. The hydrographic data sets are spatial and temporal inhomogeneous and geostrophy can be only used to describe the vertical shear of the velocity field. To get absolute velocities it is often assumed that the flow velocity vanished at some reference depth. The error made by this assumption is small near the surface where the velocities are larger than in the deep ocean where they have an order of $0.01\ \mathrm{m\,s^{-1}}$. As a consequence a small shift of the reference level can produce errors of the latter order of magnitude. In local regions where the ocean is shallower than the reference depth the bottom depth has to be chosen as reference for example.

Another possibility to calculate absolute velocities is the determination of reference velocities at the ocean surface. The velocities in the deep ocean can be calculated by vertical integration from the surface. As a second independent data set measurements from satellite altimetry can be used to determine the reference velocities.

Using numerical models for the purpose the data are accounted by assimilation techniques. The model states computed must fulfill the model equations and have to take into account the data. Properly, data assimilation denotes prognostic models. Diagnostic models where the model parameters are adapted to the data are called inverse models. An optimization approach is applied to fit the parameters. A so-called cost function is minimized in consideration of the model equality constraints. Basic concepts are described by Thacker (1988),

Olbers (1989) and Wunsch (1996). First computations with this method were made e.g. by Schröter (1989). Schröter et al. (1993) and Vogeler and Schröter (1995, 1999) applied the method to regional eddy-resolving ocean models. Schlitzer (1993, 1995) developed a box model for the Atlantic, which is extended to the global ocean (de las Heras and Schlitzer, 1999). Nechaev and Yaremchuk (1995) and Yaremchuk et al. (1998) presented an adjoint model for analyzing hydrographic sections. A global model to investigate the barotropic ocean circulation originated from Seiß (1996). Sloyan (1997) presented a box model for the Southern Ocean.

The models mentioned above are box models and/or use the finite difference method (FDM). In the present model the finite element method (FEM) is used. Originally the FEM was developed in the 1950s and 1960s to solve problems occuring in elastomechanics. Later the FEM was expanded for applications to many other physical processes which are described by partial differential equations. The theory of the FEM is described in detail for example by Zienkiewicz (1977) and Johnson (1990). There are successful applications in tidal model since the beginning of the 1970s. Examples are the works of Connor and Wang (1973), Walters and Werner (1989) and Le Provost and Vincent (1991). But there are only a few works which use the FEM in (global) circulation models. A first work was presented by Fix (1975) with a quasigeostrophic model. Haidvogel et al. (1980) compared the FEM with the FDM. For problems in fluid dynamics and particular for convection- and advection-diffusion problems the FEM became popular in the 1980s. At that time different upwind methods for stabilization were developed. A basic work is given by Brooks and Hughes (1982). In recent years Myers and Weaver (1995) used the FEM in a diagnostic barotropic ocean model. Iskandarani et al. (1995) presented a spectral finite element model

for the shallow water equations. With a similar model Haidvogel et al. (1997) described the global circulation and Wunsch et al. (1997) investigated the dynamics of long-period tides. This model was also used by Taylor et al. (1997), Levin et al. (1997) and Curchitser et al. (1998,1999). Further developments of finite element models for the shallow water equations were presented by Behrens (1996, 1998), Le Roux et al. (1998) and Giraldo (1999,2000a,2000b). Zhu et al. (1994) worked with data assimilation in a 2-dimensional finite element model for the shallow water equations.

Another finite element circulation model is QUODDY (Ip et al., 1995), which is used for regional comprehensive coastal modeling (Lynch et al., 1996). QUODDY is based on the conventional 3-dimensional shallow water equations. It is tide-resolving to investigate shelf circulation. The meshes are created by prisms and a general terrain-following vertical coordinate is used. Recently, a inverse model version of QUODDY is designed which uses an assimilation scheme like the adjoint method (Lynch and Hannah, 2000).

Altogether applications of the FEM in oceanography – especially in 3-dimensional inverse models – are still rare.

The major goal of this work is the development of an internally consistent 3-dimensional adjoint model using finite elements to investigate the large scale ocean circulation. The model solves the stationary advection-diffusion problem. A mesh is generated with tetrahedra. These elements are particular suitable to represent the complex 3-dimensional geometry given by the bottom topography. The mesh is totally unstructured so that any local refinement is possible. This is one of the great advantages of the FEM compared to the FDM. Another advantage is that the adjoint code can be created relative easy.

The model describes a flow field in geostrophic balance and conserves mass and heat.

The control variables of the inverse model are horizontal reference velocities at the ocean surface and sources (heat and fresh water fluxes) in the advection-diffusion equation. Assimilated data are among others climatologic hydrographic data and sea surface height (SSH) data from satellite altimetry.

The second major goal of this work is a first application of the model to the South Atlantic to study the large scale circulation, the formation and spreading rates of water masses and the exchange of heat and salt. The main attention directs to the Weddell Sea.

The organization of this paper is as follows: The governing model equations and the strategy of the adjoint model is described in section 2. In section 3 the use of the FEM is presented. The application of the model and its results are discussed in section 4 and 5. Finally, a summary and conclusions are given in section 6.

2 The Inverse Model

In this section the strategy of the model is presented. The model parameters are temperature T, salinity S, density ρ, velocities $\mathbf{u} = (\mathbf{u}_h, w) = (u, v, w)$ and sources F^T and F^S of the advection-diffusion equation for temperature and salinity. The density ρ is calculated from the temperature field and the salinity field with the equation of state. Using the density and a prescribed reference velocity the horizontal flow field $\mathbf{u}_h$ is computed and from that the vertical velocities w are determined considering mass conservation. Solving the advection-diffusion equations with this flow field yields new temperatures and salinities. Data are assimilated with the adjoint method in the model. A cost function J fits the model to the data and measures the quality of the model solution. The model para-

meters are divided in independent parameters – the control variables of the cost function – and in dependent parameters. We solve for a set of parameters which are minimizing the value of the cost function. This set represents a certain circulation pattern (flow field) and the corresponding temperature and salinity fields which are both in geostrophic and advective-diffusive balance.

2.1 Model Equations

The general ocean circulation is described by equations of motion which are modified Navier-Stokes equations including the effects of the rotating Earth. The fluid is only a thin stratified layer on the Earth sphere. This is taken into consideration by certain approximations. A detailed treatment and the concepts of this subject are given in the book by Gill (1982) for example. The surface circulation is mainly wind-driven but the deep circulation is determined by the gradients of pressure and density respectively. The density ρ depends on the temperature T and the salinity S of the sea-water and is given by a highly nonlinear equation of state:

$$E^{\rho} = \rho - R\ (T, S, p) = 0, \tag{1}$$

where $p = 0.1 \cdot \Delta z$ is the pressure in bar. A formula (so-called UNESCO-formula, 1981) for R is presented by Gill (1982).

For a small ratio between the nonlinear term and the Coriolis force in the equations of motions and a small aspect ratio (ratio between the characteristic depth and the characteristic length of the ocean) the horizontal flow field is described, to lowest order, by the

geostrophic equations:

$$fv = \frac{1}{\rho}\frac{\partial p}{\partial x}, \qquad\qquad fu = -\frac{1}{\rho}\frac{\partial p}{\partial y}. \tag{2}$$

There u and v are the horizontal velocities, g is the acceleration of gravity and $f = 2\Omega \sin\phi$ is the Coriolis parameter. The geostrophic approximation represents the balance between the Coriolis force and the pressure gradient. Together with the hydrostatic balance $\partial p/\partial z = -g\rho$ the thermal wind relation

$$\frac{\partial u}{\partial z} = \frac{g}{\rho f}\frac{\partial \rho}{\partial y}, \qquad\qquad \frac{\partial v}{\partial z} = -\frac{g}{\rho f}\frac{\partial \rho}{\partial x}, \tag{3}$$

can be derived which yields only the vertical shear of the flow field. On the other hand the unknown pressure field of the geostrohpic relation is now replaced by the density field which can be measured. Vertical integration of the thermal wind equations with reference to the spatially varying velocities u_{ref} and v_{ref} at the surface results in

$$\begin{aligned} E^u &= u(x,y,z) - u_{ref}(x,y) + \frac{g}{\rho f}\int_z^{-h_e} \frac{\partial \rho}{\partial y} dz' = 0, \\ E^v &= v(x,y,z) - v_{ref}(x,y) - \frac{g}{\rho f}\int_z^{-h_e} \frac{\partial \rho}{\partial x} dz' = 0. \end{aligned} \tag{4}$$

In the Ekman layer ($0 \geq z \geq -h_e$) $\mathbf{u}_h(z) = \mathbf{u}_{ref} = (u_{ref}, v_{ref})$ is valid. The vertical velocities are computed by vertical integration of the equation of continuity. The integration begins at the bottom with the kinematic boundary condition $w(-H) = \mathbf{u}_h \cdot \nabla H$ and ends at the depth $-h_e$ of the Ekman layer:

$$E^w = w(z) + \int_{-H}^{z} \left(\frac{\partial u}{\partial x} + \frac{\partial v}{\partial y}\right) dz' - w(-H) = w(z) + \nabla \cdot \int_{-H}^{z} \mathbf{u}_h dz' = 0. \tag{5}$$

The advective transport and the diffusion of the thermodynamic tracers temperature and salinity is given by the stationary advection-diffusion equation

$$\begin{aligned} E^T &= \mathbf{u} \cdot \nabla T - K_h \Delta_h T - K_v \frac{\partial^2}{\partial z^2} T - F^T = 0, \\ E^S &= \mathbf{u} \cdot \nabla S - K_h \Delta_h S - K_v \frac{\partial^2}{\partial z^2} S - F^S = 0. \end{aligned} \tag{6}$$

K_h and K_v are the horizontal and the vertical diffusion coefficients. The sources F^T and F^S are implemented to parameterizing subscale processes which are not resolved by the model because of its properties (e.g. local grid spacing).

Using this set of model equations to determine the deep circulation for a steady state is a common choice for inverse models (see Wunsch 1996).

The independent model parameters (control variables) are the horizontal reference velocities u_{ref} and v_{ref} and the sources F^T and F^S:

$$\mathbf{p} = [\ldots, u_{ref,j}, \ldots, v_{ref,j}, \ldots, F^T_j, \ldots, F^S_j, \ldots]^T. \tag{7}$$

The other horizontal velocities and the temperature T, the salinity S, the density ρ and the vertical velocities w constitute the set of dependent parameters

$$\mathbf{q} = [\ldots, u_i, \ldots, v_i, \ldots, T_i, \ldots, S_i, \ldots, \rho_i, \ldots, w_i, \ldots]^T. \tag{8}$$

The control variables $\mathbf{p}$ are initialized and varied in the inverse model part. The dependent parameters $\mathbf{q}$ are calculated from the model equations.

2.2 Cost Function

The value of the cost function J calculated from all independent and dependent parameters $\mathbf{p}$ and $\mathbf{q}$ represents the quality of the actual model state with respect to the data.

The different terms contributing to the cost function penalize unwanted properties of the model solution. The goal is to minimize the value of the cost function by driving the model solution to the preferred model state. The model solution depends highly from the characteristics of the cost function.

In this work the following terms determine the cost function:

$$
\begin{aligned}
J \;=\; \frac{1}{2} \;\Bigg[& \sum_{i,j=1}^{n_{uv}} \left(v_{ref,i} - \frac{g}{f}\frac{\partial}{\partial x}\zeta_{i,dat}\right)^T W_{ij}^{v} \left(v_{ref,j} - \frac{g}{f}\frac{\partial}{\partial x}\zeta_{j,dat}\right) && (9)\\
& + \sum_{i,j=1}^{n_{uv}} \left(u_{ref,i} + \frac{g}{f}\frac{\partial}{\partial y}\zeta_{i,dat}\right)^T W_{ij}^{u} \left(u_{ref,j} + \frac{g}{f}\frac{\partial}{\partial y}\zeta_{j,dat}\right) && (10)\\
& + \sum_{i,j=1}^{n_{F}} \left(F_i^T - F_{i,dat}^T\right)^T W_{ij}^{F_T} \left(F_j^T - F_{j,dat}^T\right) && (11)\\
& + \sum_{i,j=1}^{n_{F}} \left(F_i^S - F_{i,dat}^S\right)^T W_{ij}^{F_S} \left(F_j^S - F_{j,dat}^S\right) && (12)\\
& + \sum_{i,j=1}^{n_{w}} \left(w_i - \mathrm{curl}\left(\frac{\tau_i^w}{f_i}\right)\right)^T W_{ij}^{w} \left(w_j - \mathrm{curl}\left(\frac{\tau_j^w}{f_j}\right)\right) && (13)\\
& + \sum_{i,j=1}^{n_{T}} \left(T_i - T_{i,dat}\right)^T W_{ij}^{T} \left(T_j - T_{j,dat}\right) && (14)\\
& + \sum_{i,j=1}^{n_{S}} \left(S_i - S_{i,dat}\right)^T W_{ij}^{S} \left(S_j - S_{j,dat}\right) \;\Bigg] && (15)\\
= \quad & J_{uv} \;+\; J_F \;+\; J_w \;+\; J_T \;+\; J_S \quad .
\end{aligned}
$$

The first and the second term (9,10 – connected to J_{uv}) consider the gradient of the sea surface height (SSH) ζ. ζ_{dat} are measurements of SSH from satellite altimetry. Deviations between the SSH gradient an the corresponding reference velocities are penalized. The terms (11) and (12) lumped into J_F fit the sources F^T and F^S to F_{dat}^T and F_{dat}^S, which are zero on the whole model domain. Term J_w (13) penalizes deviations between the vertical velocities w_i at $z = -h_e$ and the curl of the wind field τ^w over f. The last two terms J_T

and J_S (14 and 15) ensure that the temperatures T and salinities S are close to the data T_{dat} and S_{dat}. The weighting matrices W_{ij} are diagonal. The diagonal elements are the inverse of the variances σ_{kk}^2 of the data.

2.3 The Adjoint Model

The main task of the model is that new model states, characterized by the set of new parameters ($\mathbf{p}_{new}$ and $\mathbf{q}_{new}$), are computed with a smaller value of the cost function J than for the actual state with parameters $\mathbf{p}$ and $\mathbf{q}$. After all the value of the cost function ought to become a minimum. A descent direction must be found in the phase space spanned by the control variables $\mathbf{p}$ so that the value of the cost function decreases. For that the gradient of the cost function ∇J is provided to an optimization algorithm. In this work a variable-storage quasi-Newton algorithm from Gilbert and Lemaréchal (1989) is used. Minimizing the cost function is an optimization problem with equality constraints which are the model equations (1 - 6). The model states have to obey the model equations exactly. A well known method to solve such problems is the method of Lagrange multipliers (see Le Dimet and Talagrand, 1986; Thacker, 1988; Schröter, 1989). The benefit is that the so-called Lagrangian function L has a stationary point in the minimum of the cost function J. The Lagrangian function L is a function of all model parameters $\mathbf{p}$ and $\mathbf{q}$ and the unknown Lagrange multipliers $\lambda = [\ldots, \lambda_j, \ldots]^T$. It reads

$$L(\mathbf{p}, \mathbf{q}, \lambda) = J + \sum_{j=1}^{n_{eq}} \lambda_j E_j \tag{16}$$

where $E_j = 0$ denote the model equations (1 - 6). n_{eq} is the number of model equations. The gradient of the Lagrangian function becomes zero at the minimum of the cost function

($\nabla L = 0$). Then all partial derivatives of L are vanishing:

$$\frac{\partial L}{\partial \lambda_j} = E_j = 0 \tag{17}$$

$$\frac{\partial L}{\partial q_i} = \frac{\partial J}{\partial q_i} + \sum_{j=1}^{n_{eq}} \lambda_j \frac{\partial E_j}{\partial q_i} = 0 \tag{18}$$

$$\frac{\partial L}{\partial p_i} = \frac{\partial J}{\partial p_i} + \sum_{j=1}^{n_{eq}} \lambda_j \frac{\partial E_j}{\partial p_i} = 0. \tag{19}$$

The derivatives with respect to the λ_j yield the model equations. The derivatives with respect to the the dependent parameters $\mathbf{q}$ and the control variables $\mathbf{p}$ (18 and 19) are called *adjoint equations*. The minimum of the cost function has to fulfill all three equations.

The optimization algorithm is an iterative process. First the Lagrange multipliers are computed from equation (18) which can be written in an n_{eq}-dimensional system of linear equations

$$\mathbf{A} \cdot \lambda + \mathbf{b} = 0 \quad \text{with} \quad A_{ij} = \frac{\partial E_j}{\partial q_i} \quad \text{and} \quad b_i = \frac{\partial J}{\partial q_i}. \tag{20}$$

This system is solved with an iterative ILU-preconditioned GMRES-solver (see Saad and Schultz, 1986; Barett et al., 1994). The Lagrange multipliers λ_j are substituted in equation (19). One obtains then the partial derivatives $\partial L/\partial p_i$ which are part of the input to the optimization procedure of Gilbert and Lemaréchal (1989).

The entire model algorithm contains the following steps:

1. Initialization of the model including the control variables $\mathbf{p}$.

2. **Forward model:** Computation of the dependent parameters $\mathbf{q}$ by solving the model equations (1 - 6).

3. Compare model parameters with data. Stop if optimum is reached.

4. **Adjoint model:**

   (a) Compute the Lagrange multipliers from the adjoint equation (18).

   (b) Compute the gradient $\nabla_{\mathbf{p}} L$ from the adjoint equation (19).

   (c) Provide the gradient $\nabla_{\mathbf{p}} L$ to the optimization algorithm and receive new improved independent parameters $\mathbf{p}_{new}$.

5. Back to step 2.

Inverse models can use several independent and synoptic data sets. Different tracer can be combined and different kinds of information can be provided to the model. Of course, the necessity to create the adjoint of the forward model is not advantageous. The large requirements of cpu-time and memory of an adjoint model is another important task.

Following from the model algorithm the density of the k-th iteration is calculated from the temperature and the salinity of the previous iteration ($\rho^k = R(T^{k-1}, S^{k-1}, p)$). This fact results in a separation of the n_{eq}-dimensional system of linear equations (20) into six subsystems with dimensions not larger than the number of nodes of the model grid.

The initialization of the model algorithm includes the computation of an initial horizontal flow field $\mathbf{u}_h$ from the geostrophic equations using an initial density field $\rho = R(T_{dat}, S_{dat}, p)$. The reference depth of the flow field is 3000 m. In regions shallower than 3000 m the local depth of the ocean is used as reference. In the Ekman layer ($z \geq -h_e$) Ekman velocities are added to $\mathbf{u}_h$.

3 The Finite Element Model

Physical processes and mathematical models of engineering are often described by partial differential equations. Only very simple cases can be treated analytically. In general it is necessary to apply numerical methods for finding approximate solutions. A common one is the finite element method (FEM) which was developed first in the 1950s and 1960s to treat problems in elastomechanics. Later the method was expanded to a lot of other physical problems.

In any numerical model the given continuous problem with infinitely many degrees of freedom is transformed to a discrete problem with a finite number of degrees of freedom. In the classical finite difference method the derivatives of a differential equation are replaced by difference quotients to obtain the discrete equations. In finite elements the discretization originates from a variational principle and uses a low order expansion of the unknown fields. The goal is that the solution of the discrete system of equations yields a sufficiently good approximation of the solution of the original continuous problem. Using the FEM to create a model to solve a given partial differential equation contains four basic steps (Johnson, 1990): (1) variational formulation of the given problem, (2) discretization of the problem with the FEM, (3) solving the discrete problem and (4) implementation of the model on a computer.

The theory and the basic concepts of the FEM are described in detail in several book like those of Zienkiewicz (1977) and Johnson (1990). Here we discuss our use of finite elements and we describe the variational formulation and the discretization (section 3.1) including stabilization (section 3.2) for the stationary advection-diffusion problem (6).

A great advantage of finite element models is that unstructured meshes can be used. The FEM is very useful to treat problems on complex geometries, which is much more difficult to deal with using finite differences. Unstructured grids are very suitable to describe the bottom topography and the coast lines of the oceanic basins. Also, any local mesh refinement is possible without increasing the number of nodes too much. 3-dimensional meshes can be generated by tetrahedra, prisms, parallelepipeds or curvilinear elements.

The variational principle includes integration by parts which results in a reduction of the order of the highest derivative to only half of the order as the derivatives of the original partial differential equation. Thus, the elements and their transition conditions can be chosen rather simple.

The parameter fields are defined continuous on the whole domain in finite elements as a superposition of the so-called basis functions. The basis functions are polynomial functions of low order. They are defined respectively on a single element in a way that they are equal to unity at one node of that element and that they are vanishing at all other nodes (see below).

An additional item interesting for inverse models is that the adjoint of the discrete equations given by the weak formulation of the variational principle are easily derived.

In this work tetrahedra (fig. 1) are the basic elements used in a totally 3-dimensional unstructured mesh. They are much more flexible in 3-d mesh generation than prisms for example and they have easy basis functions and transition conditions. Of course, the ratio between the horizontal and the vertical diameter of the tetrahedra reaches an order of magnitude up to O(100) - O(1000). However, the ratio between the scales of the horizontal and the vertical terms in the advection-diffusion equation (6) has the same order of

magnitude. A vertically stratified mesh using a 2-d unstructured mesh which is copied to each depth-level or a terrain-following vertical coordinate mesh like in QUODDY (Lynch et al., 1996) is not quite as flexible as a 3-d unstructured mesh for local refinement. In addition, a terrain-following vertical coordinate is not well suited to describe the ocean dynamics at large gradients of the topography across the shelf breaks.

3.1 The Standard Galerkin Method for Advection-Diffusion Problems

Advection-diffusion problems are occuring in many physical processes like in fluid dynamics or in transport problems. The advection-diffusion equation for any tracer $C = C(\mathbf{x}, t)$ like temperature T or salinity S is written

$$\frac{\partial C}{\partial t} + \nabla \left(\mathbf{u}(\mathbf{x}) \cdot C - K \nabla C \right) = f(\mathbf{x}), \qquad \mathbf{x} = (x, y, z) \; \epsilon \; \Omega \; \subset \; \mathbf{R}^3. \tag{21}$$

Here $\mathbf{u}$ is the velocity field and K is the diffusion coefficient. f is a source term on the right-hand side and t is the time. In the case of incompressible fluids ($\nabla \cdot \mathbf{u} = 0$) and steady states this equation simplifies to

$$\mathbf{u} \nabla C - K \Delta C = f(\mathbf{x}) \qquad \text{in } \Omega \subset \mathbf{R}^3. \tag{22}$$

This equation corresponds to the model equation (6). Here, for the sake of simplicity of description the diffusion coefficient is set to $K = K_h = K_v$. In the application of the model (see section 4) the coefficients are different and values of $K_h = 5 \cdot 10^4$ m^{2}s^{-1} and $K_v = 5 \cdot 10^{-2}$ m^{2}s^{-1}, respectively, are used.

The conditions on the boundary $\Gamma = \Gamma_1 \cup \Gamma_2$ of Ω are supposed as

$$\begin{aligned} C(\mathbf{x}) &= C_b(\mathbf{x}), \qquad \mathbf{x} \in \Gamma_1 \qquad \text{(Dirichlet conditions)} \quad \text{and} \\ K\frac{\partial C}{\partial n} &= q, \qquad\quad \mathbf{x} \in \Gamma_2 \qquad \text{(Neumann conditions).} \end{aligned} \tag{23}$$

The standard Galerkin method (SGM) (see Johnson, 1990 or Dobrindt, 1999) is the fundamental technique in finite elements when treating non-symmetric problems. The stationary advection-diffusion equation (22) is one of them.

The weak formulation in the SGM arises by multiplication of equation (22) with a so-called test function ϕ and integration over the domain Ω

$$(\mathbf{u}\nabla C, \phi) + (K\Delta C, \phi) = (f, \phi) \tag{24}$$

where the scalar product is defined by

$$(a, b) := \int_{\Omega} a \cdot b \; d\Omega. \tag{25}$$

Partial integration (1. Greens formula) is applied to get rid of higher order derivatives:

$$(\mathbf{u}\nabla C, \phi) + (K\nabla C, \nabla\phi) - K\left(\phi, \frac{\partial C}{\partial n}\right)_{\Gamma} = (f, \phi). \tag{26}$$

The index Γ means that the scalar product is integrated along the boundary Γ. Taking into consideration the boundary conditions (23) and assuming that the test functions are vanishing on Γ_1 ($\phi(\mathbf{x}) = 0$ on $\mathbf{x} \in \Gamma_1$, homogeneous boundary conditions), the weak formulation reads:

Find $C(\mathbf{x}) \in H_0^1(\Omega)$, so that

$$(\mathbf{u}\nabla C, \phi) + (K\nabla C, \nabla\phi) = (f, \phi) + (q, \phi)_{\Gamma_2} \tag{27}$$

for any $\phi(\mathbf{x}) \in H_0^1(\Omega)$. $H_0^1(\Omega)$ is the Sobolev space of functions with square integrable first derivatives in space.

In the next step the weak formulation (27) will be approximated by finite dimensional subspaces of $H_0^1(\Omega)$. Then the discrete formulation reads:

Find $C_h \, \epsilon \, V_h \; \subset \; H_0^1(\Omega)$ with

$$V_h = \{\phi \, \epsilon \, H_0^1(\Omega) \mid \phi_{h|\tau} \, \epsilon \, P_1(\tau), \; \tau \, \epsilon \, T_h\}, \tag{28}$$

so that

$$(\mathbf{u}\nabla C_h, \phi_h) + (K\nabla C_h, \nabla\phi_h) = (f, \phi_h) + (q, \phi_h)_{\Gamma_2}. \tag{29}$$

T_h is the partition of Ω in subdomains (finite elements) τ. Here the elements are tetrahedra. P_1 denotes the space of linear functions defined on the elements τ. The finite series by linear functions is sufficient because only first derivatives occur in the weak formulation. The approximated C_h are

$$C_h = \sum_{j=1}^{N} C_j \cdot \varphi_j(\mathbf{x}) + C_b, \tag{30}$$

where $C_b \, \epsilon \, H_0^1(\Omega)$ satisfies the inhomogeneous Dirichlet boundary conditions (eq. 23). N is the number of grid points given by the elements τ. The functions φ_i form a finite basis $\varphi = \{\varphi_1, \varphi_2, \ldots, \varphi_N\}$ which span the subspace V_h. They are called basis functions and satisfy the homogeneous boundary conditions. Now, any $\phi_h \, \epsilon \, V_h$ can be written as a linear combination of the φ_i:

$$\phi_h = \sum_{i=1}^{N} \phi_{h,i} \cdot \varphi_i. \tag{31}$$

Piecewise linear basis functions on the elements (tetrahedra) τ can be defined by

$$\varphi_i(\mathbf{x}) = a_i x + b_i y + c_i z + d_i, \qquad\qquad \varphi_i(\mathbf{x}_j) = \delta_{ij}, \tag{32}$$

where $\mathbf{x} \epsilon \tau$ (see Appendix). The four corner points of the tetrahedra τ are denoted by the index $i, j = 1, \ldots, 4$. The so-called global basis functions ϕ_h are expressed by the so-called local basis functions φ_i.

Using (30) in equation (29) and substituting the ϕ_h by the local basis functions φ_i, equation (29) can be written as a system of N (index i) ordinary differential equations with N unknown coefficients C_j (index j):

$$\sum_{j=1}^{N} C_j \ [(\mathbf{u} \cdot \nabla\varphi_j, \varphi_i) + (K\nabla\varphi_j, \nabla\varphi_i)] = (f, \varphi_i) + (q, \varphi_i)_{\Gamma_2} - Q_b \tag{33}$$

$$\text{with} \qquad Q_b = (\mathbf{u} \cdot \nabla C_b, \varphi_i) + K(\nabla C_b, \nabla\varphi_i) \qquad \text{and} \quad i = 1, 2, \ldots, N.$$

In the next step we have to define a representation of the current field $\mathbf{u}$. It is well known that a main problem of the FEM is the proper choice of discrete spaces to guarante the property of conservation for the discrete problem. In equation (33) the tracer C is approximated by piecewise linear basis functions. Using piecewise constant velocities $\mathbf{u} = (u, v, w)$ in conjunction with piecewise linear tracers C is a well known approximation (Thomasset, 1981; Brezzi et al., 1992). Firstly, because this set of velocities is non-divergent within each element and it simplifies the stabilization scheme (see next section). Secondly it was demonstrated (Brezzi et al., 1992) that different stabilization methods result in the well known "streamline diffusion" stabilization method, which is described below. In addition, this low order approximation minimizes the number of control variables $\mathbf{p}$ (7) and dependent model parameters $\mathbf{q}$ (8), which is an important task to limit the requirements of memory and cpu-time of the adjoint model. The piecewise constant velocities used in the advection-diffusion equation (6) are derived by projection from the piecewise linear velocities (Thomasset, 1981) given by the thermal wind equations (4) and the equation

of continuity (5). The diffusion coefficient K is also chosen piecewise constant on the elements.

Finally equation (33) can be written in the form of a system of linear differential equations:

$$\mathbf{S} \cdot \mathbf{c} = \mathbf{f}. \tag{34}$$

$\mathbf{S}$ is denoted the stiffness matrix and $\mathbf{f}$ is denoted the load vector.

$\mathbf{c} = (C_1, \ldots, C_j, \ldots, C_N)^T$ is the unknown solution vector.

3.2 Stabilization

The FEM used to be unpopular for treating advection-diffusion (convection-diffusion) problems. The reason was that numerical instabilities may occur for advection dominated flows. This is also a well-known problem when using finite differences. As a consequence various stabilization techniques (upwind-schemes) were developed. In this subsection we will have a brief look on some common techniques which turn out to be equivalent to each other for the case considered here. For more details we refer to the cited literature.

The local Péclet number Pe_τ describes the relation between the advective and the diffusive term of the advection-diffusion equation (22) in the local element τ:

$$Pe_\tau = \max\left(Pe_{\tau,h}\,,\, Pe_{\tau,v}\right) = \max\left(\frac{\parallel \mathbf{u}_h \parallel \; h_{\tau,h}}{2\; K_h}\,,\, \frac{\parallel w \parallel \; h_{\tau,v}}{2\; K_v}\right). \tag{35}$$

$h_{\tau,h}$ is the horizontal and $h_{\tau,v}$ the vertical diameter of the element τ. The flow is advective/convective dominated for large Péclet numbers.

A well known stabilization technique is the streamline upwind Petrov Galerkin method (SUPG). This method has been developed first by Brooks and Hughes (1982). Starting from equation (24) of the SGM we will use now augmented test functions $\tilde{\phi} = \phi + \psi$.

The ϕ are continuous but the ψ can be discontinuous over the boundaries of the elements. They assume the part of the upwind corrections. Following the weak formulation of the SGM the discrete equations with the upwind corrections read:

$$\begin{aligned}\Big(\mathbf{u}\nabla C_h, \phi_h\Big) + \Big(K_h \nabla_h C_h, \nabla_h \phi_h\Big) + \Big(K_v \frac{\partial}{\partial z} C_h, \frac{\partial}{\partial z}\phi_h\Big) \quad &+ \quad \sum_{\tau \epsilon T_h} \Big(\mathbf{u}\nabla C_h, \psi_h\Big)_\tau \\ = \Big(f, \phi_h\Big) \quad &+ \quad \sum_{\tau \epsilon T_h} \Big(f, \psi_h\Big)_\tau \qquad (36)\end{aligned}$$

with the scalar product $(a,b)_\tau = \int\limits_\tau a \cdot b \; d\Omega$. The summations have to be carried out over all elements τ. These terms represent a kind of artificial diffusion. For the functions ψ_h Brooks and Hughes (1982) introduced

$$\psi_h = A_\tau \; \mathbf{u} \cdot \nabla \phi_h \qquad \text{with}$$

$$A_\tau = \frac{h_{\tau,h} \; \xi(Pe_\tau)}{2 \parallel \mathbf{u}_h \parallel} \quad \text{for} \quad Pe_{\tau,h} \geq Pe_{\tau,v} \quad \text{and} \quad A_\tau = \frac{h_{\tau,v} \; \xi(Pe_\tau)}{2 \parallel w \parallel} \quad \text{otherwise.} \qquad (37)$$

There are various suggestions for the parameter ξ depending on the local Péclet number Pe_τ (Hughes et al., 1986, Franca et al., 1992):

$$\begin{aligned}\xi(Pe_\tau) &= \coth(Pe_\tau) - Pe_\tau^{-1} && \text{'optimal',} \\ \xi(Pe_\tau) &= \min\left(\tfrac{1}{3} Pe_\tau,\ 1\right) && \text{'double asymptotic',} \\ \xi(Pe_\tau) &= \max\left(0,\ 1 - Pe_\tau^{-1}\right) && \text{'critical approximation'.}\end{aligned}$$

The functional relationships for $\xi(Pe_\tau)$ show that there is no or only a small effect of the stabilization scheme for small Péclet numbers ($Pe_\tau \lesssim 1$).

Hughes et al. (1989) presented a modified version of the SUPG denoted Galerkin least-squares method (GLS). In this case the term $\nabla\phi_h$ of the function ψ_h (eq. 37) is substituted by the residuum of the advection-diffusion equation applied to the test function ϕ_h. The

function ψ_h is written then

$$\psi_h = \tilde{A}_\tau \left(\mathbf{u}\nabla\phi_h - K_h\Delta_h\phi_h - K_v\frac{\partial^2}{\partial z^2}\phi_h \right) = \tilde{A}_\tau \left(\mathbf{u}\cdot\nabla\phi_h \right). \tag{38}$$

The second and the third term in the brackets vanishes because ϕ_h is piecewise linear. In this special case ψ_h of equation (38) is equivalent to the ψ_h of equation (37) if the parameter $\tilde{A}_\tau = A_\tau$ is used.

Brezzi et al. (1992) presented another rather new stabilization technique which uses the so-called bubble functions. However, they showed as well that in the case of piecewise linear tracers and piecewise constant velocities this method is also equivalent to SUPG and GLS.

4 An Application to the South Atlantic

The model presented in section 2 and 3 is first applied to the South Atlantic. The model domain extends from 70°W to 20°E and from 30°S to 74°S. Our interest is focussed on the Weddell Sea which is embedded in the model domain.

4.1 The Mesh

The mesh is unstructured and contains 13431 nodes and 65623 tetrahedra. The grid spacing is $\leq 2°$ horizontally and ≤ 750 m in the vertical direction. There are prescribed levels in 50 m, 100 m, 200 m and 400 m. Normal to the bottom the grid spacing is smaller than 500 m. The mesh is generated with the IBG grid generator written by I. Schmelzer (1995) using ETOPO5 data (National Geophysical Data Center, 1988) for topography. The IBG generator is a grid based generator and works with a combined Octree/Delaunay

method. Figure (2) shows the bottom topography and the open boundaries of the model. The mesh yields a sparse stiffness matrix $\mathbf{S}$ with rank 13431 and $nz = 182103$ nonzero elements.

4.2 Data and Boundary Conditions

The climatologic data for temperature T_{dat} and salinity S_{dat} used in the model are data provided by the WHP Special Analysis Center (Gouretski and Jancke, 1998). Wind stress is taken from Hellerman and Rosenstein (1983). The annual mean is used for the stationary model.

The data set for the sea surface height ζ (SSH) was produced from measurements of satellite altimetry. The mean sea surface – originating from the CLS/SHOM[1] (Hernandez and Schaeffer, 2000) – is referenced to the EGM96 geoid (Lemoine et al., 1998). To reduce small scale noise of the geoid model a filtering technique according to Wahr et al. (1998) is used. The averaging kernal of the filter has a radius of 4.5°. Filtered SSH data are presented in figure (3).

The advection-diffusion equation (6) is solved for the temperature ($C = T$) and the salinity ($C = S$) on the model domain. The boundary conditions for T and S are $\partial T/\partial n = \partial S/\partial n = 0$ at the bottom. Along the open boundaries $T = T_{dat}$ and $S = S_{dat}$ is prescribed. In the regions with outflow between 0°E and South Africa along the northern boundary at 30°S (Benguela Current) and between 40°S and 60°S along the eastern boundary at 20°E (Antarctic Circumpolar Current) $\partial T/\partial n = 0$ and $\partial S/\partial n = 0$ is set as outflow conditions. The horizontal and the vertical diffusion coefficients are prescribed with $K_h = 5 \cdot 10^4$ m^{2}s^{-1}

[1]Collecte Localisation Satellites/ Service Hydrographique et Océanographic de la Marine

and $K_v = 5 \cdot 10^{-2}$ m^{2}s^{-1}. The total volume transports across the open boundaries are prescribed, too. Through the boundary along 70°W 130 Sv (1 Sv = 10^6 m^{3}s^{-1}) flow into the South Atlantic. This value is also given by Reid (1989). The same amount leaves the model domain at 20°E. The total transports across the northern and southern open boundaries vanish. Constraining the transport of the ACC to investigate the circulation in the Weddell Sea is a common practice. For example Beckmann et al. (1999) also prescribed the ACC transport through the Drake Passage with a value of 130 Sv.

4.3 Solving the Systems of Linear Equations

The model computations performed on a Cray J90 computer. The system of linear equations (34) arising from the finite element discretization of the advection-diffusion equation and the calculation of the Lagrange multipliers are solved using the GMRES-solver (Generalized Minimal RESidual, Saad and Schultz, 1986; Barett et al., 1994) of the SITRSOL routine. The SITRSOL routine is part of the scientific library (SCILIB) for Cray systems. It provides iterative solvers for real general sparse systems using preconditioned conjugate-gradient-like methods. ILU(m)-factorization (Incomplete LU) is used for preconditioning. The (integer) parameter m denotes the level of fill-in for the factorization. The amount of fill-in in the lower and the upper triangular matrices $\mathbf{L}$ and $\mathbf{U}$ is given by $2m \cdot nz$. To improve the performance of the GMRES-solver and to reduce the requirements of memory for the fill-in elements the Metis package (Karypis and Kumar, 1998) is used for reordering the coefficient matrix $\mathbf{S}$. The high quality of the reordering produced by the Metis package for our problem was demonstrated earlier by Dobrindt and Frickenhaus (2000).

5 Results

We now discuss the results of the model application to the South Atlantic. The model solution found is distinguished by reference velocities u_{ref}, v_{ref} close to those calculated from the gradient of the SSH data and by temperatures T and salinities S close to the data T_{dat} and S_{dat}. The differences between model values and hydrographic data are in the range of the errors of the hydrographic data. The deviations of the reference velocities from their equivalent are very small. First we have a look on the spreading of different water masses. Afterwards we discuss the circulation pattern of the model solution, the volume transports and the exchange of heat and salt.

5.1 Water Masses

The classification of water masses depending on the neutral density γ is the same as in Sloyan (1997): Surface Water (SW) is defined by $\gamma < 26.5$. For the Antarctic Intermediate Water (AAIW) $26.5 \leq \gamma < 27.6$ is valid. The deep water ($27.6 \leq \gamma < 28.2$) is composed of the North Atlantic Deep Water (NADW) and the Circumpolar Deep Water (CDW). The CDW flows as a part of the Antarctic Circumpolar Current (ACC) through the Drake Passage into the South Atlantic. The Antarctic Bottom Water (AABW) has a neutral density of $\gamma \geq 28.2$. The upper limit for the AABW is in agreement with Orsi et al. (1999). The AABW which is formed in the basin of the Weddell Sea (Weddell Sea Deep Water, WSDW and Weddell Sea Bottom Water, WSBW) is denser ($\gamma \geq 28.27$). But the WSDW and WSBW is modified by the lower Circumpolar Deep Water (LCDW) when it is transported to the north by the deep western boundary currents. Therefore $\gamma \geq 28.2$ is

a reasonable value for the AABW in the South Atlantic.

The figures (4 - 7) show the spreading of surface water, intermediate water, deep water and bottom water in the South Atlantic along the Greenwich meridian, 20°W, 40°W and 30°S. The solid lines represent the model solution while the distribution computed from the hydrographic data is shown in dashed lines. The agreement of the model and the data is very good. Surface water occurs only in the upper 400 m north of circa 40°S. The $\gamma = 27.6$ isosurface extends up to ∼1300 m at 30°S and reaches the ocean surface between 56°S and 60°S. The lower boundary of the deep water ranges from the ocean bottom at 30°S up to 1000 m depth at the southern boundary of the model domain. The AABW is found in the Weddell Sea below 1000 m and spreads through the deep channels of the Argentine Basin and the Cape Basin at 30°S.

5.2 The Large Scale Circulation

Figure (8) presents the reference velocity field (u_{ref}, v_{ref}). The surface circulation is smooth because it reflects the structure of the SSH data. The upper-level flow field is similar to that circulation pattern. Comparisons of the circulation of the South Atlantic with that from literature (e.g. Reid, 1989; Peterson and Stramma, 1991) show much agreement. The ACC flows through the Drake Passage in the Scotia Sea and turns to the north-east. When leaving the Scotia Sea the ACC shifts back to flow in eastern direction. The ACC flows out of the model domain at the eastern boundary between 40°S and 56°S. The Subtropical Gyre enters into the model domain across the northern boundary east of the Brazilian coast and flows as South Atlantic Current (SAC) parallel to the ACC. In the region around 6°E the SAC turns to the north and leaves the model domain.

In section 4 we have already mentioned that our major attention is directed to the Weddell Sea where the circulation forms the Weddell Gyre. The upper-level Weddell Gyre is shown in the figures (8) and (9). The southward flowing part into the Weddell Sea occurs east of 6°E. Then the current turns to the west and flows along the coast of Antarctica. The center of the gyre is at (3°W, 64°S). There is a wide part of the gyre flowing to the north with an intensification near the Antarctic Peninsula. The ACC-Weddell Gyre boundary runs along 58°S. This agrees with the schematic representation of the large scale upper-level currents in figure 1 of Peterson and Stramma (1991). The figures (10, 11 and 12) present the pattern of the Weddell Gyre in the depths of 1112 m, 3962 m and 4675 m. The gyre keeps its structure from the upper layers down to the depth. The beginning of the western boundary current which transports WSBW and WSDW respectively from the Weddell Sea Basin to the north is recognizable in 3962 m depth. At the depth of 4675 m the Weddell Sea Basin is separated from the Argentine Basin and the Cape Basin. The circulation pattern of the Weddell Gyre agrees at all depth levels with that from Reid (1989). The velocities of the Weddell Gyre decrease from 3-4 $\mathrm{cm\,s^{-1}}$ near the surface to less then 2 $\mathrm{cm\,s^{-1}}$ at the bottom. These are typical values compared to Fahrbach et al. (1994a,b).

In the upper-level circulation (fig. 8) the Falkland/Malvinas Current separates from the ACC in the Scotia Sea. This western boundary current flows along the coast of South America to the north. The Brazil Current and the so-called confluence region (Gordon, 1989) near 40°S where the Brazil Current meets the Falkland/Malvinas Current is not marked. This was expected because the SSH data contain only large scale features yielding only a smooth flow field and because of the mesh resolution in the present model

version. Near South Africa the Benguela Current and the Agulhas retroflection is only weakly represented because of the smooth SSH data. Nevertheless the Agulhas retroflection has its maximum east of 20°E. North of the Weddell Gyre the circulation is dominated by the ACC and the Subtropical Gyre. Figure (13) shows the horizontal flow field of the whole model domain in 3962 m. The Weddell Gyre at this depth was already presented in figure (11). There is a current from the Weddell Sea basin into the Argentine Basin that transports bottom water from the Weddell Sea into the Argentine Basin. Along this way the bottom water is modified by the LCDW. But the flow field in the Argentine Basin is dominated by a counterclockwise flow pattern. The reason is that the northern component of the reference velocities depending on the smooth SSH data are not large enough to produce a northward flow at the bottom.

Comparisons of the model circulation with the flow fields produced by other numerical models show also agreements. The upper-level circulation is similar to that from England and Garcon (1994) and Barnier et al. (1996). In the work of Barnier et al. (1996) a similar westward current in northern part of the Argentine Basin at 4375 m depth is presented.

5.3 Transports

As mentioned before the total volume transports across the open boundaries are prescribed. However, the transports of the different water masses described in paragraph 5.1 are model results. They are presented in figure (14). Through the Drake Passage 38.2 Sv intermediate water (IW), 87.7 Sv deep water (DW) and 4.1 Sv bottom water (BW) are flowing into the South Atlantic. 0.2 Sv SW, 44.1 Sv IW, 70.3 Sv DW and 15.4 Sv BW are exported into the Indian Ocean across 20°E. Across the northern open boundary of the model at 30°S 4.1 Sv

SW and 20.4 Sv AAIW are transported to the north which is compensated by a southward flow of 23.6 Sv NADW. The transport of 0.9 Sv AABW to the south is due to the deep flow field in this region which has the wrong direction as we have discussed above. A closer inspection shows its characteristic as modified bottom water with $28.2 \leq \gamma < 28.27$. The northward spreading of denser bottom water with $\gamma \geq 28.27$ extends up to about 35°S which is in agreement with Orsi et al. (1999). 13.0 Sv of this water mass are formed in the Weddell Sea. These are exported totally across 20°E. The formation rate of AABW with a neutral density of $\gamma \geq 28.2$ over the whole model domain is 10.4 Sv. Rintoul (1991) estimated a formation rate of 9 Sv in his standard case and 13 Sv in the 'warm-water-path' case. Other values from by previous studies are 12.3 Sv (de las Heras and Schlitzer, 1999; study B), 5 Sv (Matano and Philander, 1993) and 1 Sv (Sloyan and Rintoul, 2000). In the work of Macdonald (1995) no bottom water production is detected. Additional estimates of AABW formation rates of previous studies are in the range from 2-15 Sv (see Table 3 in Orsi et al., 1999).

These transports result in a heat transport of 0.64 PW across 30°S to the north. This value is compared with the heat transports presented in previous studies in figure (15). The heat transports across 70°W and 20°E amount to 1.06 PW and 1.25 PW. The ratio between the transports of intermediate and deep water together with the heat transports across the open boundaries compares well with the 'warm-water-path' case of Rintoul (1991). In that study the total volume transports across 32°S, 68°W and 20°E are likewise 0 Sv, 129 Sv and 130 Sv. The heat transport across 32°S is assumed to be 0.69 PW (the value given by Hastenrath, 1982), which results in a transport of 22 Sv NADW across 30°S to the south. The heat transports across 68°W and 20°E are 1.3 PW and 1.12PW. The export

of bottom water into the Indian Ocean amounts to 16 Sv. A transport of surface water into the South Atlantic across this section like the 13 Sv in Rintoul's work is absent in our model results.

The transports of salt are 4628 $\mathrm{kt\,s^{-1}}$ eastwards across 70°W, 4631 $\mathrm{kt\,s^{-1}}$ eastwards across 20°E and 13 $\mathrm{kt\,s^{-1}}$ across 30°S to the south. The heat and salt transport across the southern open boundary at 74°S are nearly vanishing.

5.4 Vertical Velocities and Sources

Figure (16) shows the vertical velocity field w in 100 m depth. The order of magnitude of w is 10^{-6} $\mathrm{m\,s^{-1}}$. This is in good agreement with vertical velocities presented by Olbers and Wenzel (1989) and Schlitzer (1995). For clarity only the zero and the $1.0 \cdot 10^{-6}$ $\mathrm{m\,s^{-1}}$ contour lines are printed. Regions with $w < -2.0 \cdot 10^{-6}$ $\mathrm{m\,s^{-1}}$ occur south-west of South Africa and eastern of 35°W in the Weddell Sea. Western of 35°W w increases up to $6.0 \cdot 10^{-6}$ $\mathrm{m\,s^{-1}}$. Near the cost of South America we find a small area around 45°S where the vertical velocity is in the range between $\pm 8.0 \cdot 10^{-6}$ $\mathrm{m\,s^{-1}}$. The maximum value of $14.0 \cdot 10^{-6}$ $\mathrm{m\,s^{-1}}$ occurs at the Antarctic Peninsula.

The distribution of the sources F^T and F^S of the advection-diffusion equation (6) yields a pattern with no regular structure. Changes of sign are frequent. The strength of the sources increases near the bottom especially in the vicinity of steep gradients in the model topography. In such regions tetrahedra have small volumes to get a mesh close to the topography. As an example figure (17) shows the sources field along 20°W.

6 Summary and Conclusions

In this study we have presented a new adjoint model with finite elements applied to a stationary advection-diffusion problem. The usage of the finite element method (FEM) is still rare in ocean modeling. As shown in section 3 the FEM is very suitable to treat problems on complex geometries given by the coast lines and the bottom topography. It provides the possibility to work with structured or unstructured grids and local refinement. The weak formulation of the variation principle (Standard Galerkin Method, section 3.1) reduces the order of the partial differential equation by integration by parts, so that one can use simple basis functions. Different stabilization techniques for advective problems are well known (section 3.2). The adjoint equations are given by the transpose of the stiffness matrix and by derivatives of the stiffness matrix.

We presented a first application of the new model to the South Atlantic with the major attention directed to the Weddell Sea. We assimilated climatological hydrographic data and SSH data from satellite altimetry in the model. The transports of the model solution across the open boundaries agree with the values from literature. The heat transport of 0.64 PW across 30°S to the north connected with a southward transport of 23.6 Sv NADW corresponds to the 'warm-water-path' case of Rintoul's study (1991). The formation rate of bottom water with a neutral density of $\gamma \geq 28.2$ in the model domain amounts to 10.4 Sv. The upper-level circulation corresponds to that from literature. Similarly the circulation of the Weddell Gyre is in good agreement over the full depth of the Weddell Sea to that from literature. Bottom water formed in the Weddell Sea is transported to the east and to the north where it is modified by the lower CDW of the ACC.

The southward transport of 0.9 Sv bottom water ($28.2 \leq \gamma < 28.27$) at 30°S is in disagreement with literature. The main reason is that in this region the northern components of the reference velocities fitted to the gradient of the SSH data are too small to yield a northward transport at the bottom. Another important reason is the resolution of the mesh near the bottom at 30°S. It is somewhat coarser than in the Weddell Sea and there can be also some influence from open boundary effects. There are possibilities for mesh refinement but they are always limited by the large memory requirements of adjoint models. Parallelizing the model code can help here in the future.

The sources F^T and F^S of the advection-diffusion equation were introduced to parameterize subscale processes which are not resolved by the mesh and by the diffusion coefficients K_v and K_h. Constant diffusion coefficients on the whole mesh created by tetrahedra with a large range of volumes are describing the processes on the elements only roughly. In the further development of the model diffusion coefficients which are varying spatially could be suitable.

Acknowledgments: We would like to thank I. Schmelzer from the Weierstraß-Institute of Applied Analysis and Stochastics in Berlin, Germany who let us use the 3D version of the IBG grid generator and we thank two anonymous reviewers who provided many useful suggestions that helped to improve the manuscript.

Appendix

The Basis Functions

Equations (32) in paragraph 3.1 introduced the piecewise linear (local) basis functions

$$\varphi_i(x, y, z) = a_i x + b_i y + c_i z + d_i. \tag{39}$$

Four basis functions φ_i are defined on each tetrahedron. Let $i, j = 1, 2, 3, 4$ denote the corner points of the tetrahedron. Then each function φ_i is equal to 1 at the corner $i = j$, zero at all other corners and linear inbetween. The coefficients a_i, b_i, c_i and d_i are easily calculated from the coordinates $\mathbf{x}_j$ of the corner points j. For instance the first basis function $\varphi_{j=1}(x, y, z)$ of the tetrahedron τ_m reads

$$\varphi_1(x, y, z) = \frac{\alpha(x - x_3) + \beta(y - y_3) + \gamma(z - z_3)}{6 \cdot V_{\tau_m}} \tag{40}$$

where

$$\begin{aligned} \alpha &= (y_4 - y_3)(z_2 - z_3) + (y_3 - y_2)(z_4 - z_3) \\ \beta &= (x_2 - x_3)(z_4 - z_3) + (x_4 - x_3)(z_3 - z_2) \\ \gamma &= (x_2 - x_3)(y_3 - y_4) + (x_4 - x_3)(y_2 - y_3). \end{aligned}$$

The volume of the tetrahedron is

$$V_{\tau_m} = \frac{1}{6} \cdot \begin{vmatrix} x_1 - x_2 & y_1 - y_2 & z_1 - z_2 \\ x_1 - x_3 & y_1 - y_3 & z_1 - z_3 \\ x_1 - x_4 & y_1 - y_4 & z_1 - z_4 \end{vmatrix}. \tag{41}$$

References

Barett, R., M. Berry, T.F. Chan, J. Demmel, J. Donato, J. Dongarra, V. Eijkhout, R. Pozo, C. Romine und H. Van der Vorst, 1994: *Templates for the Solution of Linear Systems: Building Blocks for Iterative Methods*. SIAM, Philadelphia, PA.

Barnier, B., P. Marchesiello and A.P. de Miranda, 1996: Modelling the Ocean Circulation in the South Atlantic: A Strategy for Dealing with Open Boundaries. *The South Atlantic: Present and Past Circulation*. G. Wefer, W.H. Berger, G. Siedler, D.J. Webb, Ed., Springer-Verlag,189-304.

Beckmann, A., H. Hellmer and R. Timmermann, 1999: A Numerical Model of the Weddell Sea: Large Scale Circulation and Water Mass Distribution. *J. Geophys. Res.*, **104**(C10),23375-23391.

Behrens, J., 1996: *Adaptive Semi-Lagrange-Finite-Elemente-Methode zur Lösung der Flachwassergleichungen: Implementierung und Parallelisierung*. Reports on Polar Research, Alfred-Wegener-Institut, Bremerhaven, No. 217.

Behrens, J., 1998: Atmospheric and ocean modeling with an adaptive finite element solver for the shallow-water equations. *Appl. Num. Math.*, **26**,217-226.

Brezzi, F., M.-O. Bristeau, L.P. Franca, M. Mallet and G. Rogé, 1992: A relationship between stabilized finite element methods and the Galerkin method with bubble functions. *Comp. Meth. in Appl. Mech. and Eng.*, **96**,117-129.

Brooks, A.N. and T.J.R. Hughes, 1982: Streamline upwind/Petrov-Galerkin formulations for convection dominated flows with particular emphasis on the incompressible Navier-

Stokes equations. *Comp. Meth. in Appl. Mech. and Eng.*, **32**,199-259.

Connor, J.J. and J.D. Wang, 1973: Finite-element modeling of hydrodynamic circulation. *Numerical Methods Fluids Dynamics*. Pentech Press, London, 355-387.

Curchitser, E., M. Iskandarani and D.B. Haidvogel, 1998: A spectral element solution of the shallow-water equations on multiprocessor computers. *J. Atm. Oc. Tech.*, **15**(2),510-521.

Curchitser, E., D.B. Haidvogel and M. Iskandarani, 1999: On the transient adjustment of a mid-latitude abyssal ocean basin with realistic geometry: The constant depth limit. *Dyn. Atmos. Oceans.*, **29**,147-188.

Dobrindt, U., 1999: *Ein Inversmodell für den Südatlantik mit der Methode der finiten Elemente*. Alfred-Wegener-Institute for Polar and Marine Research, Bremerhaven and University of Bremen, Germany, PHD thesis, 131pp.

Dobrindt, U. and S. Frickenhaus, 2000: *Partitioning, Reordering and Solving an Advection Diffusion Problem Formulated in Finite Elements*. Department of Physics, Report 98; Alfred-Wegener-Institute, Bremerhaven, Germany.

England, M.H. and V.C. Garcon, 1994: South Atlantic circulation in a world ocean model. *Ann. Geophysicae*, **12**,812-825.

Fahrbach, E., G. Rohardt, M. Schröder and V. Strass, 1994a: Transport and structure of the Weddell Gyre. *Ann. Geophysicae*, **12**,840-855.

Fahrbach, E., M. Schröder and A. Klepikov, 1994b: Circulation and Water Masses in the Weddell Sea. *Phys. of Ice-Covered Seas*, **2**,569-604.

Fix, G.J., 1975: Finite element model for ocean circulation problems. *SIAM J. Appl. Math.*, **29**(3),371-387.

Franca, L., S.L. Frey and T.J.R. Hughes, 1992: Stabilized finite element methods: I. Application to the advective-diffusive model. *Comp. Meth. in Appl. Mech. and Eng.*, **95**,253-276.

Fu, L.-L., 1981: The general circulation and meridional heat transport of the subtropical South Atlantic determind by inverse methods. *J. Phys. Oceanogr.*, **11**,1171-1193.

Gilbert, J.C. and C. Lemaréchal, 1989: Some Numerical Experiments with Variable-Storage Quasi-Newton Algorithms. *Mathematical Programming*, **45**,407-435.

Gill, A.E., 1982: *Atmosphere-Ocean Dynamics*. Academic Press, Inc..

Giraldo, F.X., 1999: Trajectory Calculations for Spherical Geodesic Grids in Cartesian Space. *Monthly Weather Rev.*, **127**,1651-1662.

Giraldo, F.X., 2000a: Lagrange-Galerkin Methods on Spherical Geodesic Grids: The Shallow Water Equations. *J. Comp. Phys.*, **160**,336-368.

Giraldo, F.X., 2000b: The Lagrange-Galerkin Method for the 2D Shallow Water Equations on Adaptive Grids. *J. Num. Meth. Fluid.*, **33**,789-832.

Gordon, A.L., 1989: Brazil-Malvinas Confluence – 1984. *Deep Sea Res.*, **36**,359-384.

Gouretski, V.V. and K. Jancke, 1998: *WOCE Report No. 162/98*. WHP Special Analysis Center; Technical Report No.3 (`http://www.dkrz.de/~u241046`).

Haidvogel, D.B., A.R. Robinson and E.E. Schulman, 1980: The accuracy, efficiency and stability of three numerical models with application to open ocean problems. *J. Comput. Phys.*, **34**,1-53.

Haidvogel, D.B., E. Curchitser, M. Iskandarani, R. Hughes and M. Taylor, 1997: Global Modeling of the Ocean and Atmosphere Using the Spectral Element Method. *Numerical Methods In Atmospheric And Ocean Modelling*, C.A. Lin, R. Laprise and H. Ritchie,Ed., Canadian Meteorology and Oceanographic Society, 505-531.

Hastenrath, S., 1980: Heat budget of tropical ocean and atmosphere. *J. Phys. Oceanogr.*, **10**,159-170.

Hastenrath, S., 1982: On meridional heat transports in the World Ocean. *J. Phys. Oceanogr.*, **12**,922-927.

Hellerman, S. and M. Rosenstein, 1983: Normal Monthly Wind Stress Over the World Ocean with Error Estimates. *J. Phys. Oceanogr.*, **13**,1093-1104.

de las Heras, M. and R. Schlitzer, 1999: On the importance of intermediate water flows for the global ocean overturning. *J. Geophys. Res.*, **104**(C7),15515-15536.

Hernandez, F. and P. Schaeffer, 2000: *Altimetric Mean Sea Surfaces and Gravity Anomaly maps Inter comparisons.* AVISO technical report, No. AVI-NT-011-5242-CLS. CLS Editor, Toulouse, France.

Hughes, T.R.J., M. Mallet and A. Mizukami, 1986 A new finite element formulation for computational fluid dynamics: II. beyond SUPG. *Comp. Meth. in Appl. Mech. and Eng.*, **54**,341-355.

Hughes, T.R.J., L.P. Franca and G.M. Hulbert, 1989 A new finite element formulation for computational fluid dynamics: VIII. The Garlerkin/least-squares method for advective-diffusive equations. *Comp. Meth. in Appl. Mech. and Eng.*, **73**,173-189.

Ip, J.T.C. and D.R. Lynch, 1995: *Comprehensive Coastal Circulation Simulation using Finite Elements: Nonlinear Prognostic Time-Stepping Model. QUODDY3 User's Manual*. Report NML95-1, Dartmouth College, Hanover, NH, USA, 45pp.

Iskandarani, M., D.B. Haidvogel and J.P. Boyd, 1995: A Staggered Spectral Finite Element Method for the Shallow Water Equations. *Int. J. of Num. Meth. in Fluids*, **20**,393-414.

Johnson, C., 1990: *Numerical solution of partial differential equations by the finite element method*. Cambridge University Press.

Karypis, G. and V. Kumar, 1998: `METIS`– *A Software Package for Partitioning Unstructured Graphs, Partitioning Meshes and Computing Fill-Reducing Orderings of Sparse Matrices (Version 4.0)*. University of Minnesota, Department of Computer Science/Army HPC Research Center, Minneapolis.

Le Dimet and O. Talagrand, 1986: Variational algorithms for analysis and assimilation of meteorological observations: theoretical aspects. *Tellus*, **38A**,97-110.

Lemoine, F.G. et al., 1998: *The Development of the Joint NASA GSFC and National Imagery and Mapping Agency (NIMA) Geopotential Model EGM96*. National Aeronautics and Space Administration and Goddard Space Flight Center, NASA/TP—1998–206861.

Le Provost, C. and P. Vincent, 1991: Finite Element for modelling ocean tides. *Tidal Hydrodynamics*, B. Parker, Ed., John Wiley and sons Inc., 41-60.

Le Roux, D.Y., A. Staniworth and C.A. Lin, 1998: Finite Elements for Shallow Water Equations Ocean Models. *Monthly Weather Report*, **126**,1931-1951.

Levin, J.G., M. Iskandarani and D.B. Haidvogel, 1997: A spectral filtering procedure for eddy-resolving simulations with a spectral element ocean model. *J. Comp. Phys.*, **137**,130-154.

Lynch, D.R., J.T.C. Ip, C.E. Naimie and F.E. Werner, 1996: Comprehensive coastal circulation model with application to the Gulf of Maine. *Cont. Shelf Res.*, **16**,875-906.

Lynch, D.R. and C.G. Hannah, 2000: Inverse Model for Limited-Area Hindcasts on the Continental Shelf. submitted to *J. Atm. Oc. Tech.*, 54pp.

Macdonald, A.M., 1995: *Oceanic fluxes of mass, heat and freshwater: A global estimate and perspective*. Mass. Inst. of Technol./Woods Hole Oceanogr. Inst. Joint Program, Cambridge, PHD thesis, 326pp.

Matano, R.P. and S.G.H. Philander, 1993: Heat and Mass Balances of the South Atlantic Ocean Calculated From a Numerical Model. *J. Geophys. Res.*, **98**(C1),977-984.

Myers, P.G. and A.J. Weaver, 1995: A Diagnostic Barotropic Finite-Element Ocean Circulation Model. *J. Atm. Oc. Tech.*, **12**,511-526.

National Geophysical Data Center, 1988: *Digital Relief of the Surface of the Earth.* Data Announcement 88-MGG-02, NOAA, Boulder, CO.

Nechaev, D.A. and M.I. Yaremchuk, 1995: Application of the adjoint technique to processing of a standard section data set: World Ocean Circulation Experiment section S4 along 67°S in the Pacific Ocean. *J. Geophys. Res.*, **100**(C1),865-879.

Olbers, D., 1989: A geometrical interpretation of inverse problems. *Oceanic Circulation Models: Combining Data and Dynamics*, D.L.T. Anderson and J. Willebrand, Ed., Kluwer Academic Publishers, 79-93.

Olbers, D. and M. Wenzel, 1989: Determining diffusivities fom hydrographic data by inverse methods with applications to the circumpolar current. *Oceanic Circulation Models: Combining Data and Dynamics*, D.L.T. Anderson and J. Willebrand, Ed., Kluwer Academic Publishers, 95-139.

Orsi, A.H., G.C. Johnson and J.L. Bullister, 1999: Circulation, mixing and production of Antarctic Bottom Water. *Prog. Oceanog.*, **43**,55-109.

Peterson, R.G. and L. Stramma, 1991 Upper-level circulation in the South Atlantic Ocean. *Prog. Oceanog.*, **26**,1-73.

Reid, J.L., 1989: On the total geostrophic circulation of the South Atlantic Ocean: Flow patterns, tracers and transports. *Prog. Oceanog.*, **23**,149-244.

Rintoul, S.R., 1991: South Atlantic interbasin exchange. *J. Geophys. Res.*, **96**,2675-2692.

Saad, Y. and M.H. Schultz, 1986: GMRES: A Generalized Minimal Residual Algorithm for Solving Nonsymmetric Linear Systems. *SIAM J. Sci. Stat. Comput.*, **7**(3),856-869.

Schlitzer, R., 1993: Determining the mean, large-scale circulation of the Atlantic with the adjoint method. *J. Phys. Oceanogr.*, **23**(9),1935-1952.

Schlitzer, R., 1995: *An adjoint model for the determination of the mean oceanic circulation, air-sea fluxes and mixing coefficients.* Reports on Polar Research, Alfred-Wegener-Institut, Bremerhaven, No. 156.

Schmelzer, I., 1995: *3D Grid Generation with Contravariant Geometry Description*. Weierstrass-Institut für angewandte Analysis und Stochastik, Berlin, PHD thesis, 103pp.

Schröter, J., 1989: Driving of non-linear time-dependent ocean models by observation of transient tracers - A problem of constrained optimization. *Oceanic Circulation Models: Combining Data and Dynamics*, D.L.T. Anderson and J. Willebrand, Ed., Kluwer Academic Publishers, 257-285.

Schröter, J., U. Seiler und M. Wenzel, 1993: Variational assimilation of GEOSAT data into an eddy resolving model of the Gulf Stream extension area. *J. Phys. Oceanogr.*, **23**(5),925-953.

Seiß, G., 1996: *Ein inverses Modell der globalen barotropen Zirkulation des Ozeans*. Alfred-Wegener-Institute for Polar and Marine Research, Berichte aus dem Fachbereich Physik, Report 72, PHD thesis, 102pp.

Semtner, A.J. and R.M. Chervin, 1988: A simulation of the global ocean circulation with resolved eddies. *J. Geophys. Res.*, **93**,15502-15522.

Semtner, A. J. and R. M. Chervin, 1992: Ocean general circulation from a global eddy-resolving model. *J. Geophys. Res.*, **97**,5493-5550.

Sloyan, B., 1997: *The Circulation of the Southern Ocean and the adjacent ocean basins determined by inverse methods*. Institute of Antarctic and Southern Ocean Studies, University of Tasmania, PHD thesis, 468pp.

Sloyan, B.M. and S.R. Rintoul, 2000: The Southern Ocean limb of the global deep overturning circulation. *J. Phys. Oceanogr.*, in press.

Taylor, M., J. Tribbia and M. Iskandarani, 1997: The spectral element method for the shallow water equations on the sphere. *J. Comp. Phys.*, **130**(1),92-108.

Thacker, W.C., 1988: *Three lectures on fitting numerical models to observations.* Technical Report GKSS 87/E/65, GKSS-Forschungzentrum Geesthacht.

Thomasset, F., 1981: *Implementation of Finite Element Methods for Navier-Stokes Equations.* Springer-Verlag New York Inc..

Vogeler, A. and J. Schröter, 1995: Assimilation of satellite altimeter data into an open ocean model. *J. Geophys. Res.*, **100**(C8),15951-15963.

Vogeler, A. and J. Schröter, 1999: Fitting a regional ocean model with adjustable open boundaries to TOPEX/POSEIDON data. *J. Geophys. Res.*, **104**(C9),20789-20799.

Wahr, J., M. Molenaar and F. Bryan, 1998: Time Variability of the Earth's Gravity Field: Hydrological and Oceanic Effects and Their Possible Detection Using GRACE. *J. Geophys. Res.*, **103**(B12),30205-30299.

Walters, R.A. and F.E. Werner, 1989: A comparison of two finite element models of tidal hydrodynamics using a North Sea data set. *Adv. Water Resources*, **12**,184-193.

Webb, D.J. et al., 1991: Using an eddy resolving model to study the Southern Ocean. *EOS*, **72**,15 pages.

Wunsch, C., 1996: *The Ocean Circulation Inverse Problem.* Cambridge University Press.

Wunsch, C., D.B. Haidvogel and M. Iskandarani, 1997: Dynamics of the long-period tides. *Prog. Oceanog.*, **40**(1-4),81-108.

Yaremchuk, M., D. Nechaev, J. Schröter and E. Fahrbach, 1998: A dynamically consistent analysis of circulation and transports in the southwestern Weddell Sea. *Annales Geophysicae*, **16**, 1024-1038.

Zhu, K., I.M. Navon and X. Zou, 1994: Variational Data Assimilation with a Variable Resolution Finite-Element Shallow-Water Equations Model. *Monthly Weather Review*, **122**,946-965.

Zienkiewicz, O.C., 1977: *The Finite Element Method*. McGraw-Hill Book Company (UK) Ltd., England.

Figure captions

Figure 1: Tetrahedra are the basic elements used in this work.

Figure 2: The mesh: Bottom topography and open boundaries.

Figure 3: SSH data in m.

Figure 4: Water masses along the Greenwich meridian.

Figure 5: Water masses along 20°W.

Figure 6: Water masses along 40°W.

Figure 7: Water masses along 30°S.

Figure 8: Reference velocities (u_{ref}, v_{ref}) in the South Atlantic with South America at the north-west corner, the Antarctic Peninsula at the south-west corner, Antarctica at the south-east corner and South Africa at the north-east corner.

Figure 9: The Weddell Gyre in 100 m with the Antarctic Peninsula at the South-West and Antarctica at the South-East.

Figure 10: The Weddell Gyre in 1112 m.

Figure 11: The Weddell Gyre in 3962 m.

Figure 12: The Weddell Gyre in 4675 m.

Figure 13: Horizontal flow field in 3962 m of the South Atlantic.

Figure 14: Transports in Sv of surface water (SF, $\gamma < 26.5$), intermediate water (IW, $26.5 \leq \gamma < 27.6$), deep water (DW, $27.6 \leq \gamma < 28.2$) and bottom water (BW, $\gamma \geq 28.2$) across the open boundaries of the model domain at 30°S, 74°S, 20°E and 70°W; negative sign denotes transports to the west or to the south.

Figure 15: Comparison of the heat transports from different studies across 30°S in the

South Atlantic.

Figure 16: Vertical velocities w in $\cdot 10^{-7}\mathrm{ms}^{-}1$ in 100 m of the South Atlantic.

Figure 17: Sources F^T and F^S along 20°W. The zero-contour line is dotted.

Figures

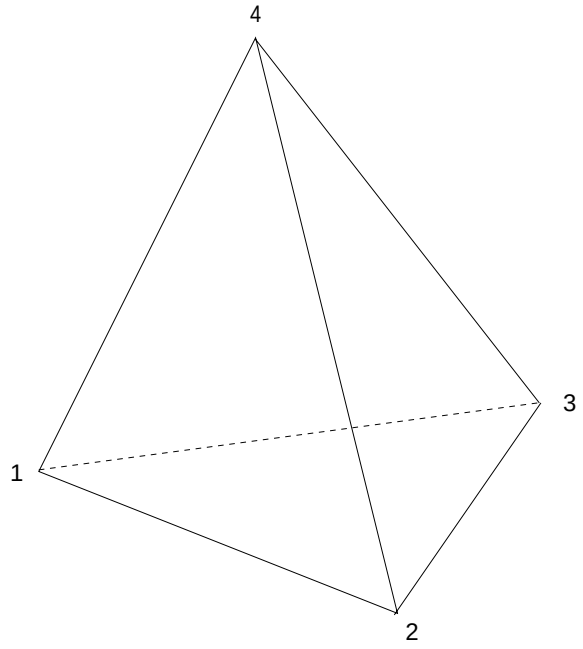

Figure 1:

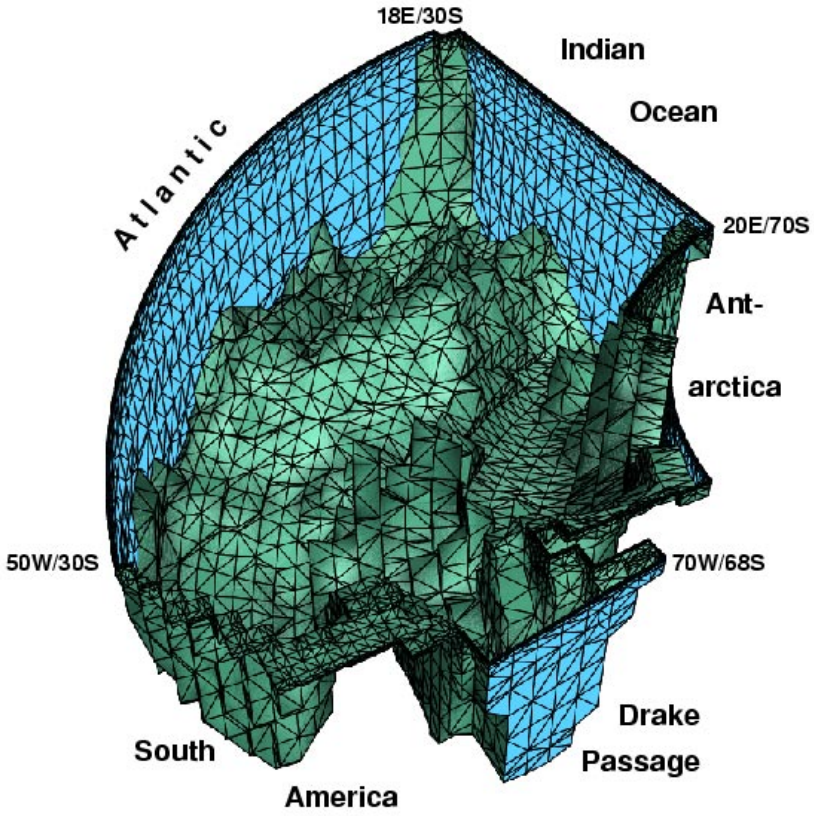
18E/30S
Indian
Ocean
Atlantic
20E/70S
Ant-
arctica
50W/30S
70W/68S
Drake
Passage
South
America

Figure 2:

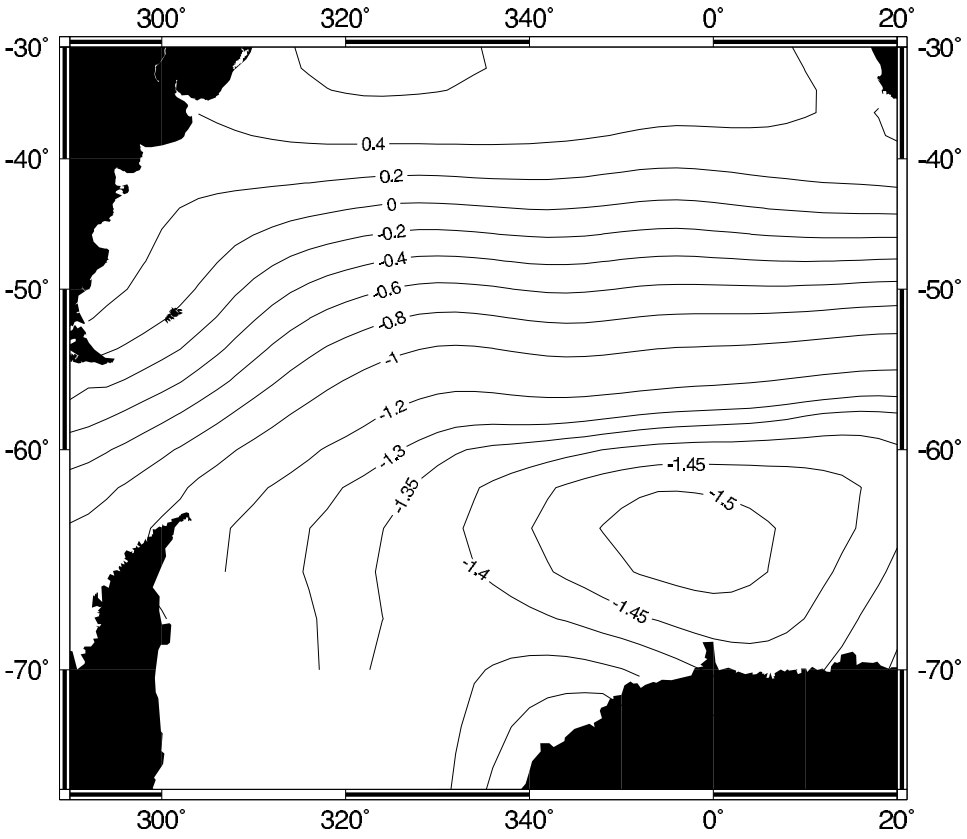
300˚
320˚
340˚
0˚
20˚
-30˚
-40˚
-50˚
-60˚
-70˚
0.4
0.2
0
-0.2
-0.4
-0.6
-0.8
-1
-1.2
-1.3
-1.35
-1.4
-1.45
-1.5

Figure 3:


neutral density γ along 0° W − data (− −), model (−)
0
−1000
−2000
−3000
−4000
−5000
−6000
depth in m
26.5
intermediate water
27.6
deep water
bottom water
28.2
−70
−65
−60
−55
−50
−45
−40
−35
−30
latitude

Figure 4:

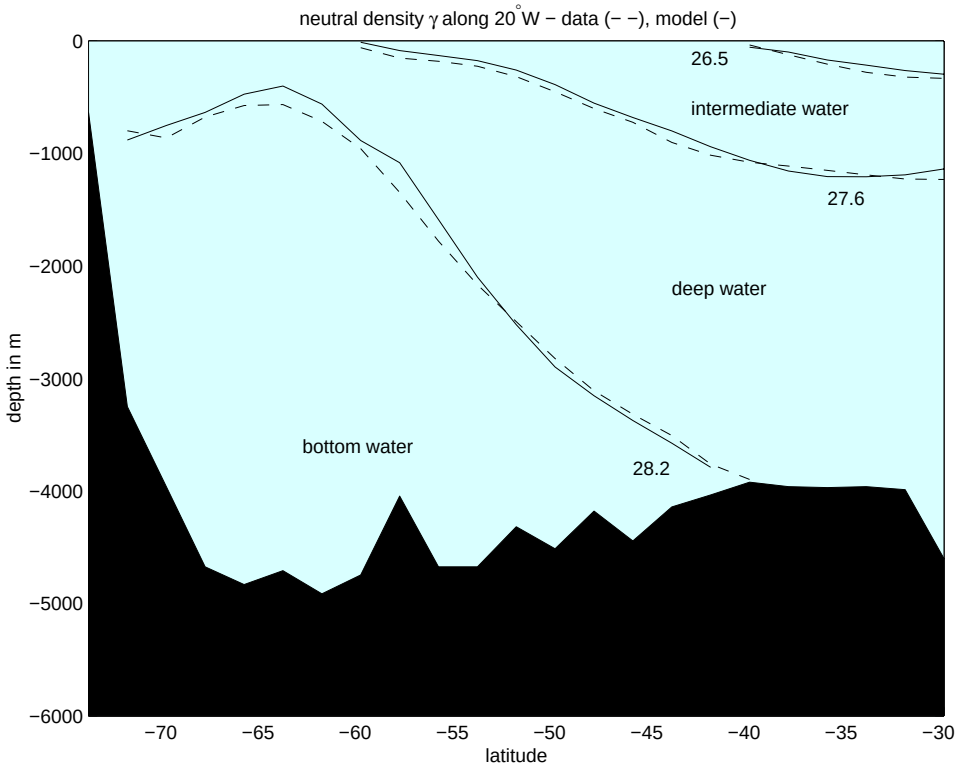
neutral density γ along 20°W − data (− −), model (−)
0
−1000
−2000
−3000
−4000
−5000
−6000
depth in m
26.5
intermediate water
27.6
deep water
bottom water
28.2
−70
−65
−60
−55
−50
−45
−40
−35
−30
latitude

Figure 5:

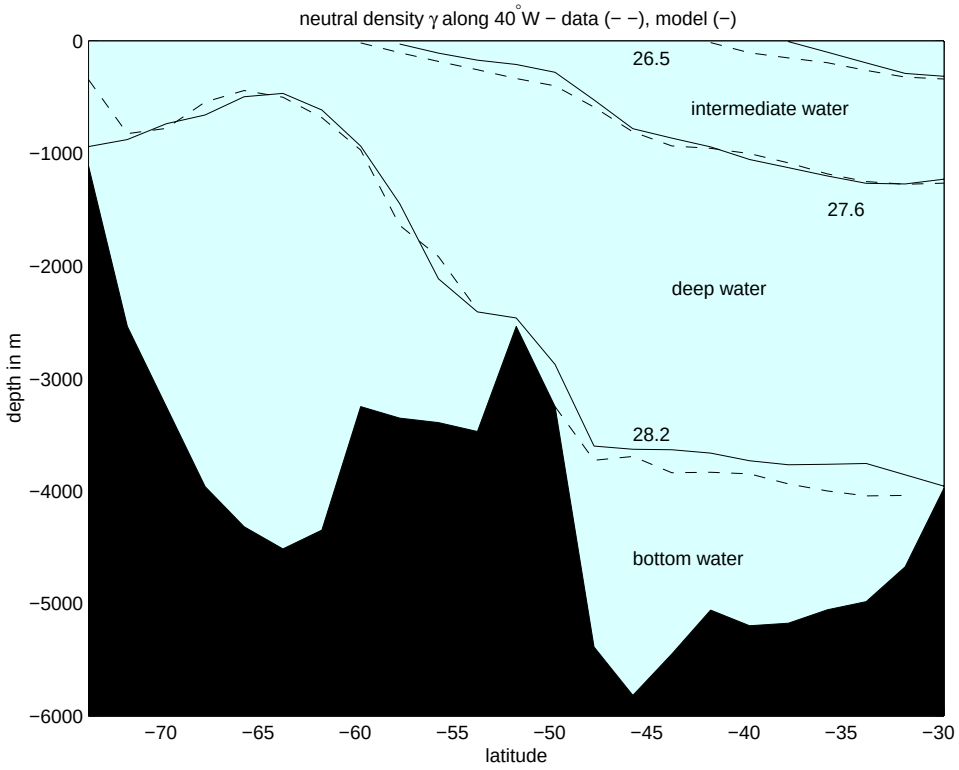
neutral density γ along 40°W − data (− −), model (−)
0
−1000
−2000
−3000
−4000
−5000
−6000
depth in m
26.5
intermediate water
27.6
deep water
28.2
bottom water
−70
−65
−60
−55
−50
−45
−40
−35
−30
latitude

Figure 6:

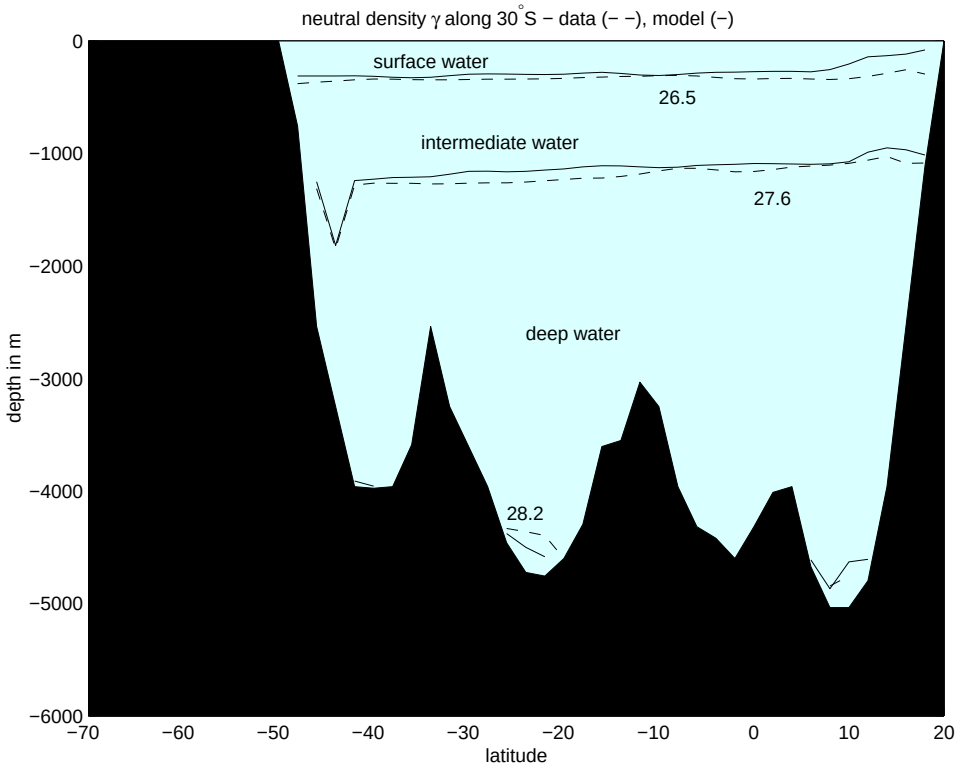
neutral density γ along 30°S − data (− −), model (−)
surface water
26.5
intermediate water
27.6
deep water
28.2
depth in m
0
−1000
−2000
−3000
−4000
−5000
−6000
−70
−60
−50
−40
−30
−20
−10
0
10
20
latitude

Figure 7:

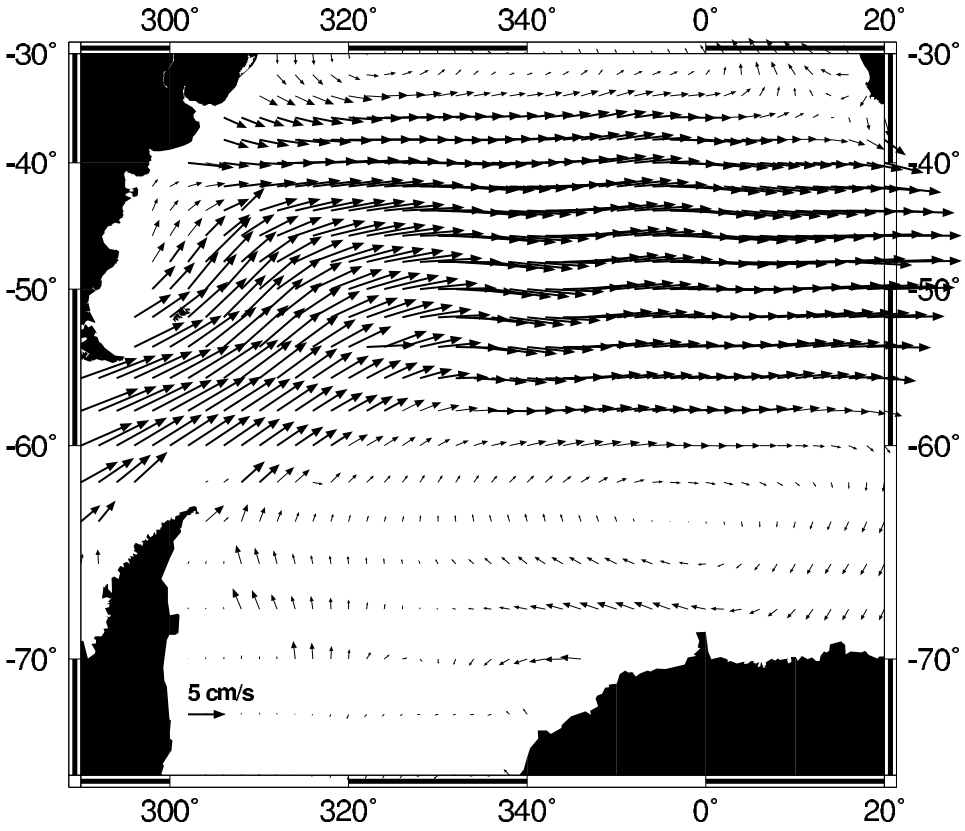

Figure 8:

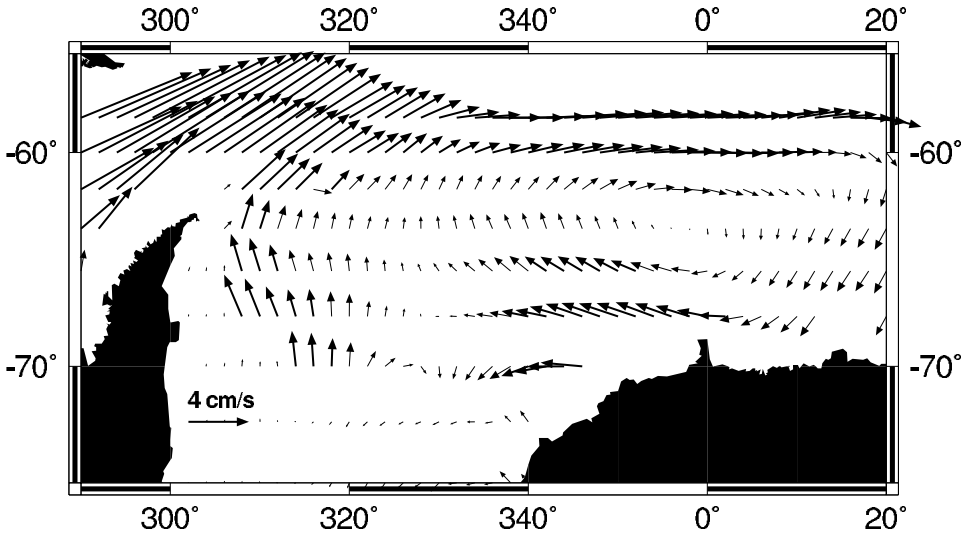

Figure 9:

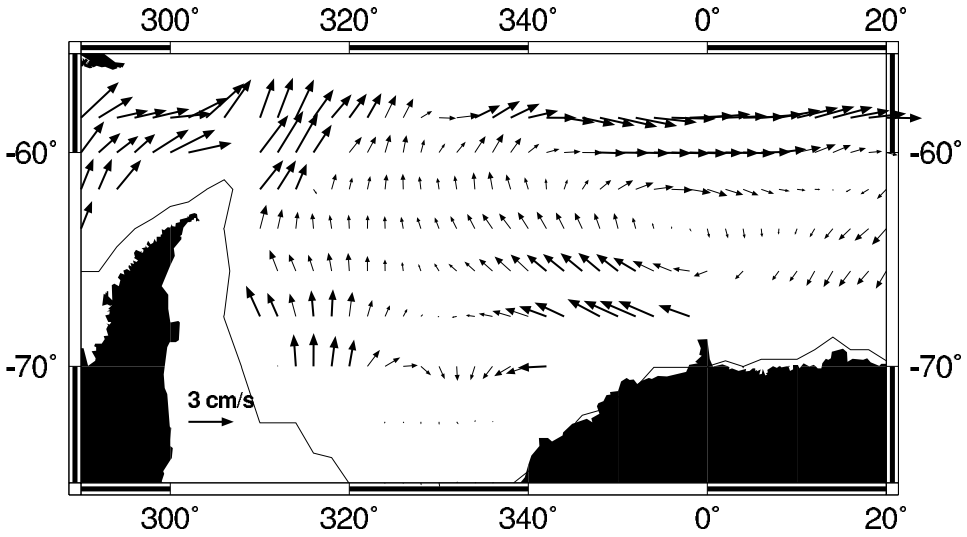

Figure 10:

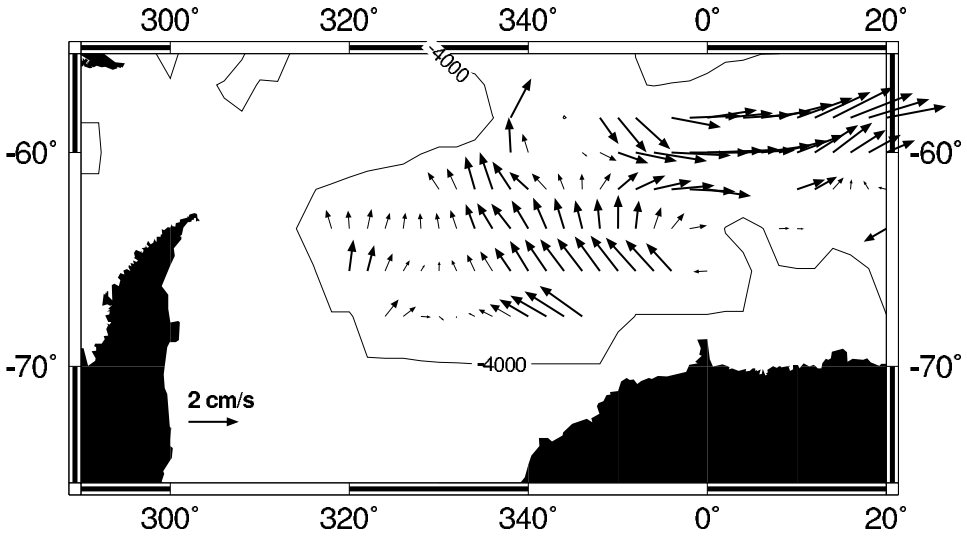

Figure 11:

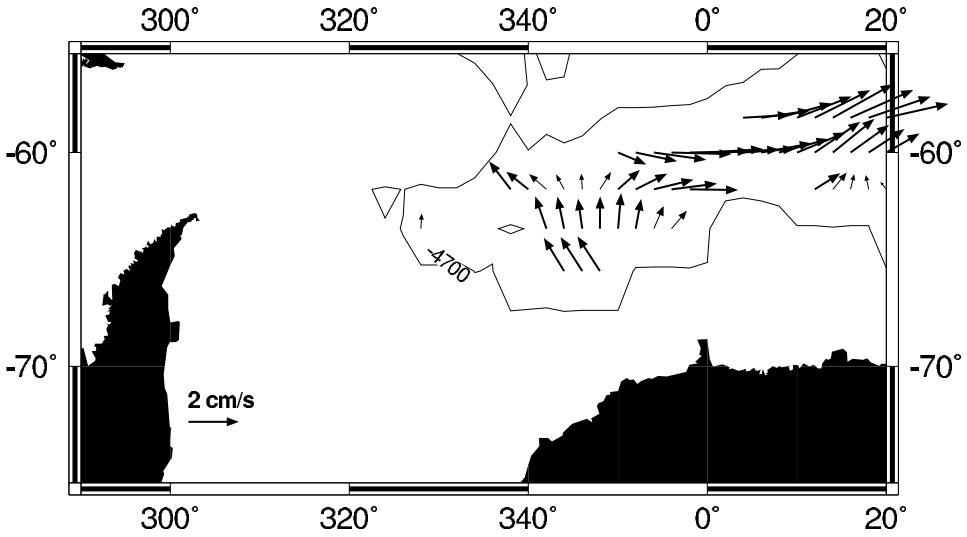

Figure 12:

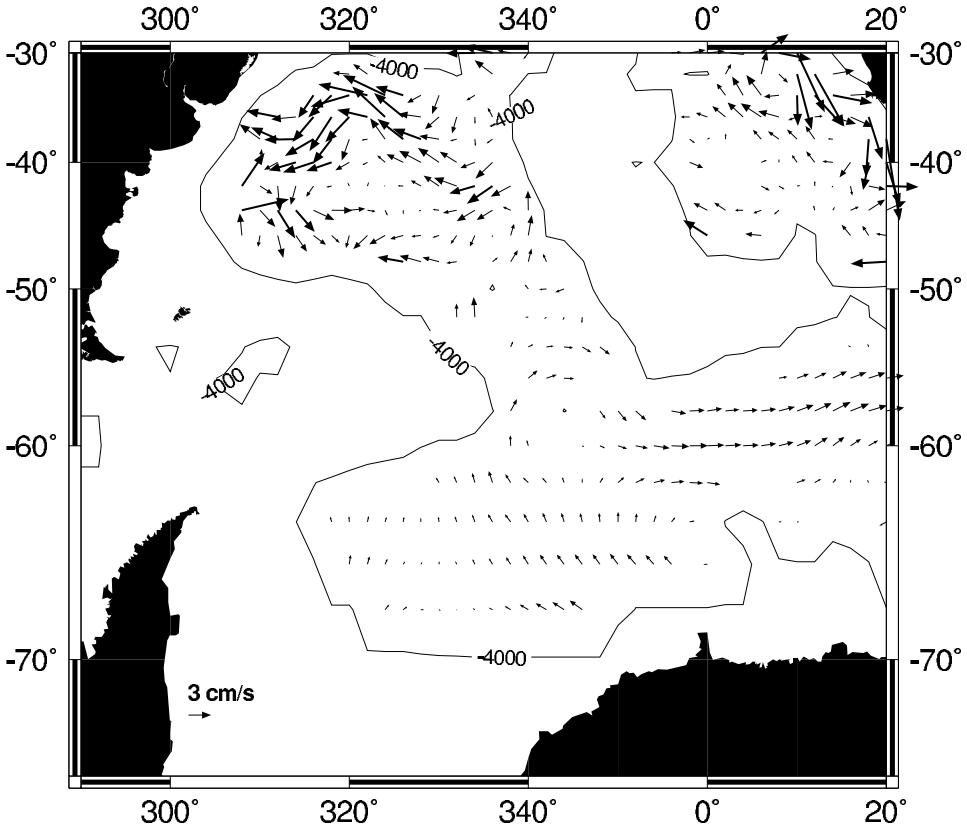

Figure 13:

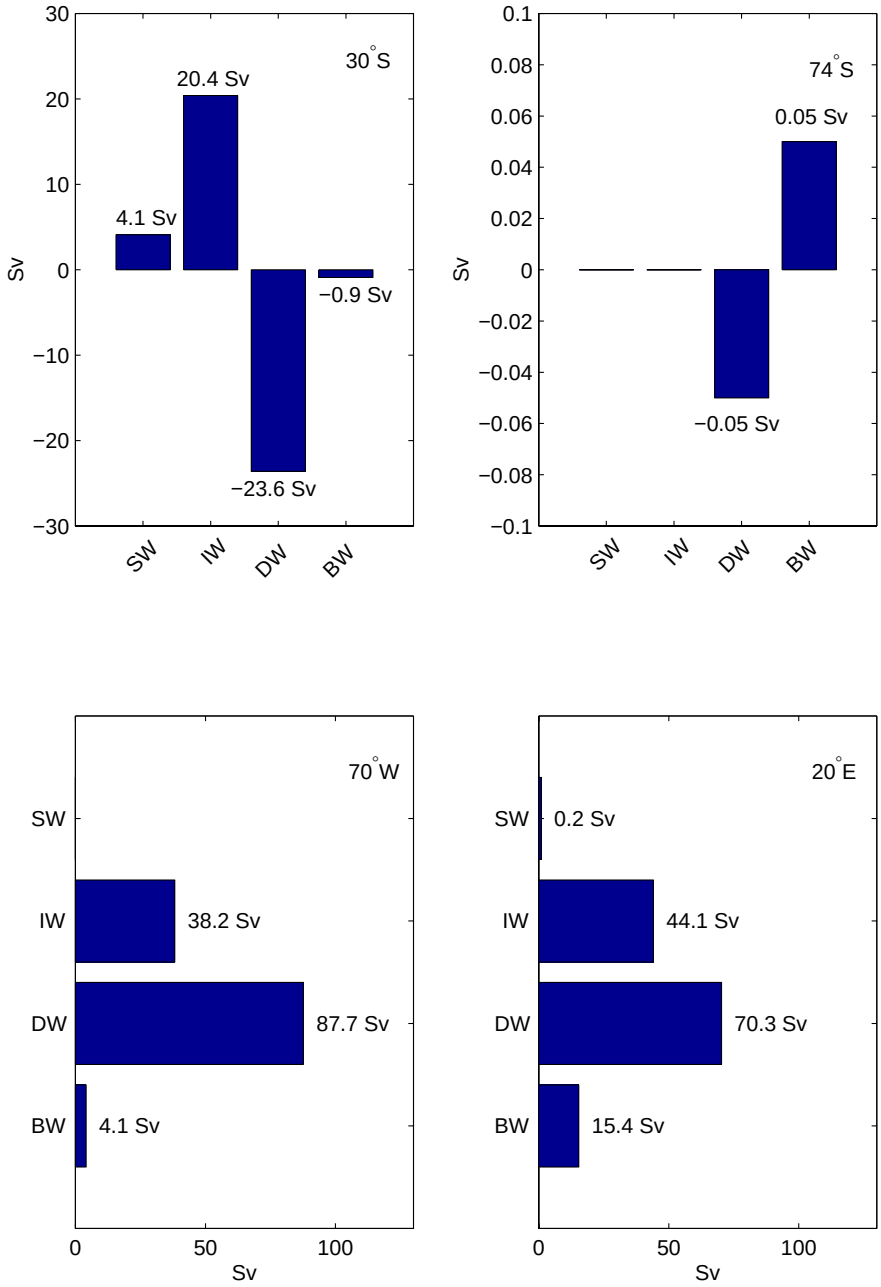
30°S
20.4 Sv
4.1 Sv
−23.6 Sv
−0.9 Sv
Sv
SW
IW
DW
BW
74°S
0.05 Sv
−0.05 Sv
70°W
38.2 Sv
87.7 Sv
4.1 Sv
20°E
0.2 Sv
44.1 Sv
70.3 Sv
15.4 Sv

Figure 14:

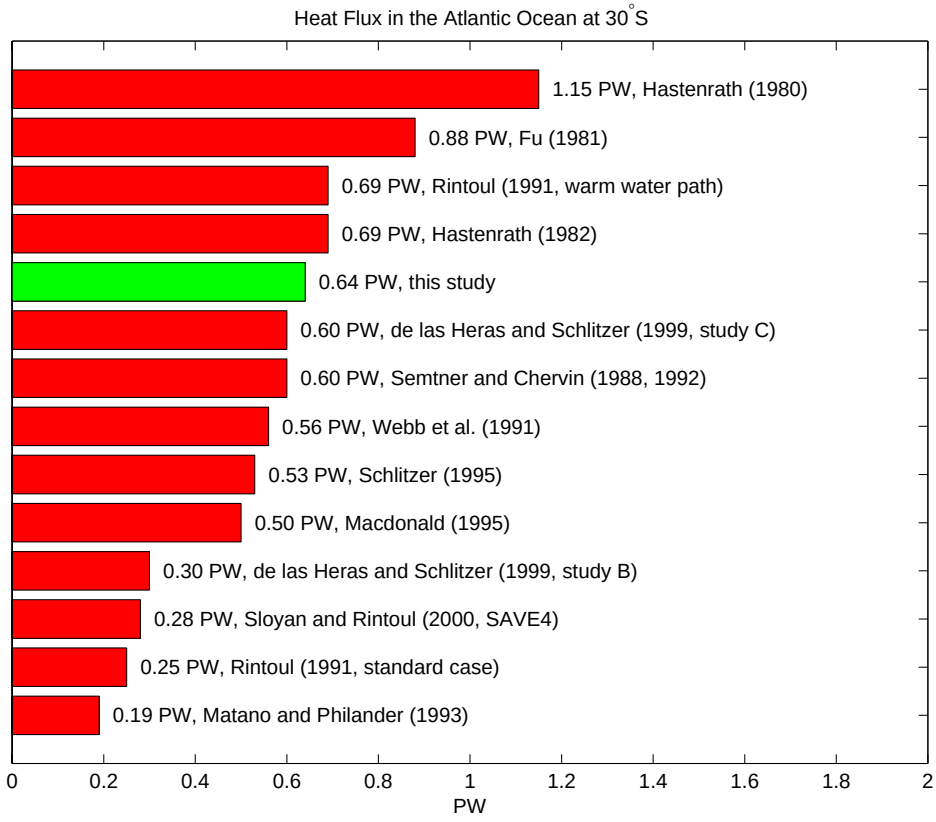
Heat Flux in the Atlantic Ocean at 30°S
1.15 PW, Hastenrath (1980)
0.88 PW, Fu (1981)
0.69 PW, Rintoul (1991, warm water path)
0.69 PW, Hastenrath (1982)
0.64 PW, this study
0.60 PW, de las Heras and Schlitzer (1999, study C)
0.60 PW, Semtner and Chervin (1988, 1992)
0.56 PW, Webb et al. (1991)
0.53 PW, Schlitzer (1995)
0.50 PW, Macdonald (1995)
0.30 PW, de las Heras and Schlitzer (1999, study B)
0.28 PW, Sloyan and Rintoul (2000, SAVE4)
0.25 PW, Rintoul (1991, standard case)
0.19 PW, Matano and Philander (1993)
0
0.2
0.4
0.6
0.8
1
1.2
1.4
1.6
1.8
2
PW

Figure 15:

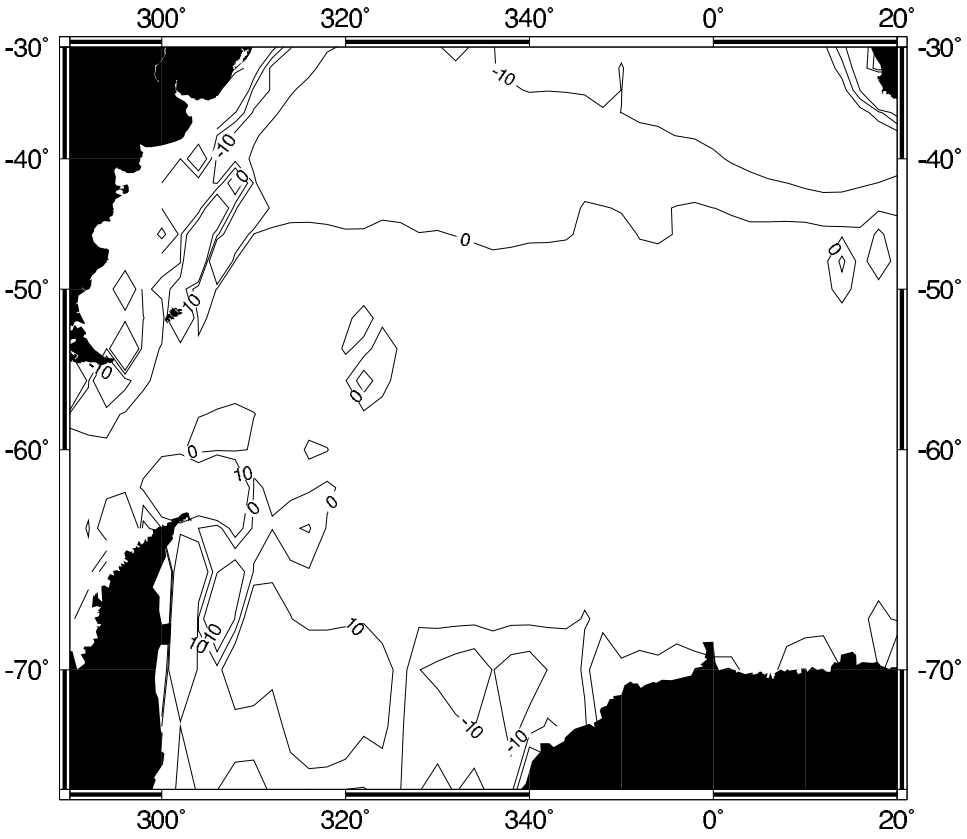

Figure 16:

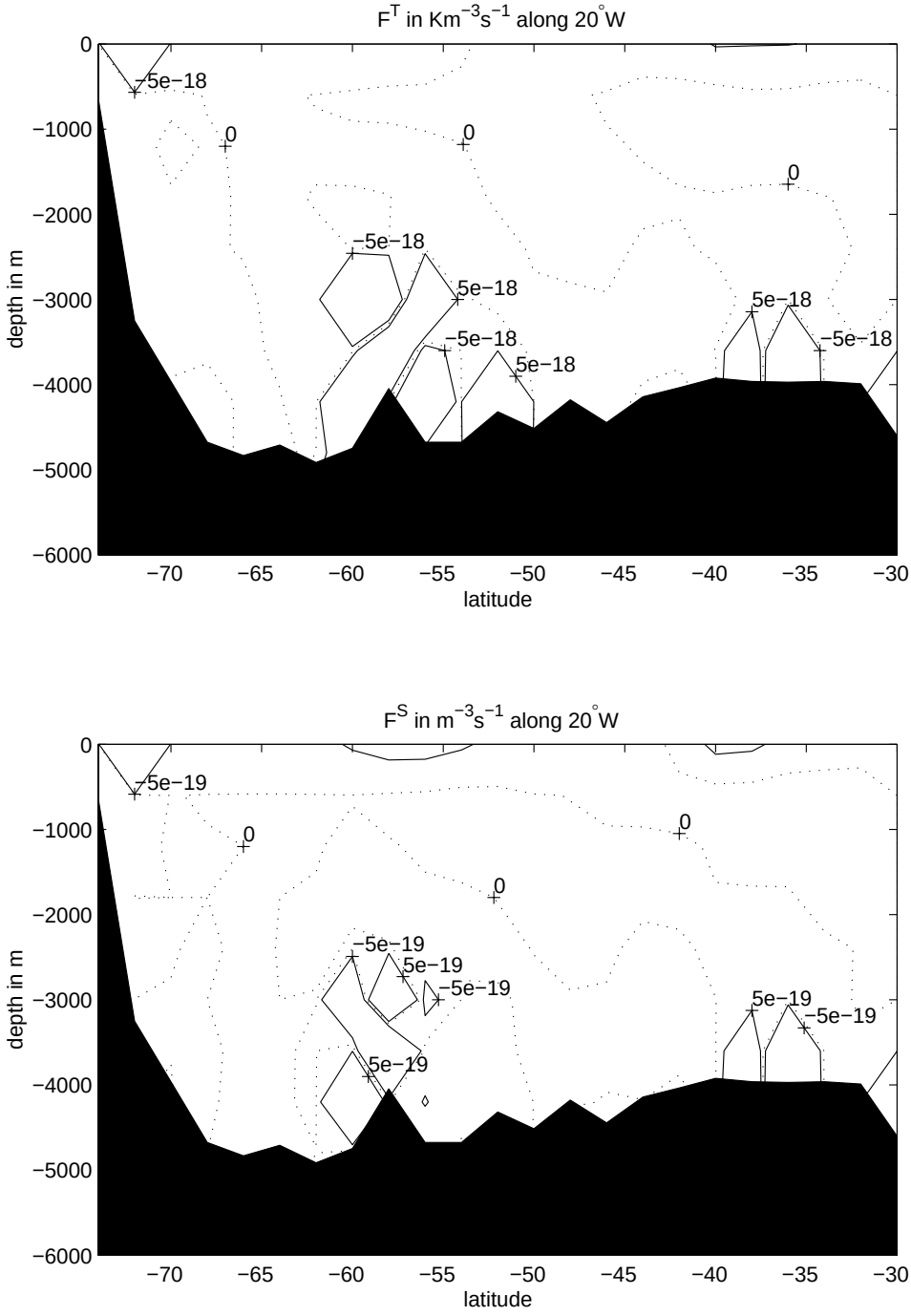
F^T in Km^−3 s^−1 along 20°W
depth in m
latitude
0
−1000
−2000
−3000
−4000
−5000
−6000
−70
−65
−60
−55
−50
−45
−40
−35
−30
−5e−18
0
5e−18
F^S in m^−3 s^−1 along 20°W
−5e−19
5e−19

Figure 17: